Guidance in the Hybrid Cardiovascular Procedure for Ventricular Septal Defect Closure

by

Gerardo TIBAMOSO PEDRAZA

THESIS PRESENTED TO ÉCOLE DE TECHNOLOGIE SUPÉRIEURE
IN PARTIAL FULFILLMENT FOR THE DEGREE OF
DOCTOR OF PHILOSOPHY
Ph.D.

MONTREAL, FEBRUARY 21, 2022

ÉCOLE DE TECHNOLOGIE SUPÉRIEURE
UNIVERSITÉ DU QUÉBEC

BOARD OF EXAMINERS

THIS THESIS HAS BEEN EVALUATED

BY THE FOLLOWING BOARD OF EXAMINERS

Mr. Luc Duong, Thesis supervisor
Department of Software and IT Engineering, École de technologie supérieure

Ms. Sylvie Ratté, Thesis Co-Supervisor
Department of Software and IT Engineering, École de technologie supérieure

Mr. Joaquim Miró, Thesis Co-Supervisor
Cardiology, Department of Pediatrics, CHU Sainte Justine

Mr. Mohamed Cheriet, Chair, Board of Examiners
Department of Systems Engineering, École de technologie supérieure

Mr. Simon Drouin, Member of the Jury
Department of Software and IT Engineering, École de technologie supérieure

Ms. Elodie Lugez, External Independent Examiner
Deparment of Computer Science, Ryerson University

THIS THESIS WAS PRESENTED AND DEFENDED

IN THE PRESENCE OF A BOARD OF EXAMINERS AND THE PUBLIC

ON JANUARY 25, 2022

AT ÉCOLE DE TECHNOLOGIE SUPÉRIEURE

ACKNOWLEDGEMENTS

The achievements presented in this thesis have been possible thanks to many people. I would like to start by mentioning that professor Luc Duong has been mentoring me with patience and perseverance; he provided me with confidence to thrive in my training as a researcher. Under their supervision, professors Sylvie Ratté and Luc Duong gave me the opportunity to come to Canada to pursue my doctoral studies. Their support has been key for my personal and professional development. Thank you, profe Luc, thank you, profe Sylvie.

This thesis was inspired and developed thanks to the insights provided by Dr. Joaquim Miró and Dr. Marie-Josée Raboisson. As experienced cardiologists, Dr. Joaquim and Dr. Marie-Josée shared with me their medical knowledge and clinical experience to understand the heart complexities. Thanks to them, I had the opportunity to attend to several cardiac interventions in pediatric patients, including a hybrid procedure to close ventricular septal defects. Additionally, Francisco, Iñaki, and Victor, residents of cardiology and working with Dr. Joaquim and Dr. Marie-Josée, supported me for data collection, analysis of diagnostic images, and testing our proposed solutions. Dr. Chantale Lapierre provided me with helpful comments to improve the Thesis' manuscript. Nathalie, Dr. Miró's secretary, also helped me in administrative duties. To all of you, thank you very much.

Thank you, Professor Elodie Lugez, Professor Simon Drouin, and Professor Mohamed Cheriet, for accepting the invitation to be part of the board of examiners of this thesis.

We used tools and equipment from different labs of the École de technologie supérieure (ETS) for the experimentation in different stages of this thesis. The technical staff in charge of those labs supported me during this endeavor, considerably. Among them: Patrice, Samuel, Thomas, Alain, and Olivier, from the département de génie logiciel et des TI; Hugo and Rachid, from the service des enseignements généraux; Radu, Nabil, and Michel, from the département de génie mécanique; Sébastien and Juan Mauricio, from the département de génie de la construction; and Rigoberto and Jorge, from the département de génie électrique. To all of you, thank you very much.

As a member of the LIVE/LiNCS lab, I have been benefited with the support and experience of my colleagues. Among them: Ruben, Ruth, Veronica, Vu, Erick, Edgar, Laura, Arlen, Xavier, Rémi, Fariba, Atefeh, Alpa, Mellie, Kuldeep, Jihen, Faten, Binh, Hilary, Bashar, Neda, Helmi, Eric, Eddie, Houda, Lina, Amlin, Amin, Frederic, Simon, Otilia, and Renzo. In our lab, I also had the opportunity to work with Sarah Amouri, Sarah Alohali, Sasha, Basudha, and Colin, in their respective internships related in some way with this thesis. The fact that we came from different countries made the interaction between us an enriching experience. To all of you, thank you very much.

The initial contacts to start my doctoral studies in Canada were made thanks to Liliana Guedez, Jorge Prieto, and Felipe Gerlein, who worked for the Service des relations internationales at ÉTS and visited Colombia at that time. They provided me advice at every step required for the immigration and the ÉTS registration processes. During the studies, Eric Nolet provided me with administrative support for my ÉTS stay abroad scholarship for a research stay at the Universidad Nacional Autónoma de México (UNAM), in Mexico City. In Mexico, I had the opportunity to meet Professor Fernando Arámbula, Professor Boris Escalante, Professor Jimena Olveres, Erika, Vivian, Fabian, and more members of the Laboratorio Avanzado de Procesamiento de Imágenes (LAPI). Additionally, Toño, Abraham, and Eric were key for accommodation in Mexico City, which is a huge city that I had not visited before. I am deeply grateful for all the support and advice that I received from all of you. Thank you very much.

My motivations to pursue doctoral studies in Canada included enriching my academic experience and improving my language skills. But perhaps the main motivation was broadening my view of the world. Nevertheless, it implied to depart and to stay away from my relatives, to whom I ask forgiveness for being absent for too long. I am deeply grateful for the constant support that I received from my parents Olga and Alfredo, my sister Miryam, my brothers Edgar and Fernando, my nephews and nieces, my aunts and uncles, my cousins, and my friends. I hope to be able to give back all the love that I received from all of you. Thank you very much.

Last but not least, this thesis was developed thanks to the financial support provided by Synchromedia lab, ÉTS; ÉTS internal scholarships for PhD candidates; ÉTS scholarship for research stay abroad; Fonds de recherche du Québec - Nature and technologies (FRQNT), doctoral research scholaships program (File 276451); and Natural Sciences and Engineering Research Council of Canada (NSERC) Discovery Grants.

Guidage dans la procédure cardiovasculaire hybride pour la fermeture de la cloison ventriculaire

Gerardo TIBAMOSO PEDRAZA

RÉSUMÉ

Les communications interventriculaires (CIV) sont des trous entre les cavités ventriculaires qui perturbent le processus normal d'oxygénation du sang. Les CIV sont des malformations cardiaques congénitales courantes qui se referment généralement d'elles-mêmes; toutefois, les communications interventriculaires de grande taille nécessitent un traitement chirurgical. Une procédure hybride vise à implanter des occludeurs pour fermer les CIV à cœur battant, étant moins invasive que la chirurgie à cœur ouvert la plus courante. La procédure est surveillée par échocardiographie transoesopagienne (ETO). L'ETO fournit des images en temps réel à des fréquences d'images élevées; néanmoins, l'ETO offre un champ de vision limité qui entrave la manœuvre des instruments chirurgicaux à l'intérieur du cœur. Par conséquent, une grande expérience est nécessaire pour interpréter les images de l'ETO et pour manœuvrer les instruments chirurgicaux. Cependant, les simulateurs médicaux pour la formation à la procédure hybride sont limités; par conséquent, la pratique directement sur les patients pourrait rester la seule alternative.

L'objectif principal de cette thèse était de fournir des solutions au problème d'assistance à la navigation pour la procédure hybride de fermeture des CIV. Cet objectif est développé au travers de trois contributions: premièrement, une méthode pour concevoir des fantômes cardiaques avec des CIV pour l'imagerie échographique; deuxièmement, une méthode de guidage de navigation pour accéder aux CIV pour l'implantation d'occludeurs; et troisièmement, un suivi du mouvement cardiaque dans les images échographiques du cœur avec CIV.

Notre première contribution s'est attaquée au problème du manque de modèles cardiaques pour l'expérimentation. Pour résoudre ce problème, nous avons développé une méthode permettant de construire des fantômes cardiaques avec des CIV pour la palpation, la ponction et l'acquisition d'images ultrasonores. Nous nous sommes appuyés sur des images provenant de cas rétrospectifs pour représenter avec précision l'anatomie cardiaque de patients pédiatriques présentant des CIV. Nous avons fabriqué des fantômes cardiaques dans deux matériaux: le silicone et le cryogel d'alcool polyvinylique (PVA-C); nous avons constaté que le PVA-C avait la meilleure échogénicité, ce qui était important pour la caractérisation des CIV en échocardiographie. Nous pensons que cette contribution fournit des outils supplémentaires pour maîtriser l'exploration des CIV pour la procédure hybride.

Notre deuxième contribution s'est attaquée au problème du champ de vision limité de l'ETO pour le guidage dans la procédure hybride. Pour le guidage de la procédure, nous avons introduit un modèle virtuel tridimensionnel (3-D) du cœur du patient et un système de mesure électromagnétique (EMS) pour suivre les instruments chirurgicaux. Nous avons validé une méthode d'enregistrement des points de repère comprenant des fantômes cardiaques, des modèles cardiaques virtuels et l'EMS dans un dispositif expérimental que nous avons développé pour

simuler la procédure hybride. Un groupe de cardiologues a effectué la procédure hybride sur les fantômes cardiaques, en manœuvrant les instruments chirurgicaux selon les informations fournies par les cœurs virtuels. Nous avons constaté que les modèles de cœurs virtuels fournissaient des informations précises pour guider l'accès aux CIV. Nous pensons que cette contribution est une preuve de concept réussie d'un système qui pourrait fournir un guidage dans une procédure hybride, en complément de l'ETO, pour accéder en toute sécurité aux CIV.

Jusqu'à présent, nous fournissons des informations de guidage dans un cœur statique. Dans un cas réel, cependant, le cœur bat. Par conséquent, notre troisième contribution s'est attaquée au problème du suivi du mouvement du cœur dans les images ultrasonores, avec une application potentielle pour synchroniser les informations de guidage (deuxième contribution) avec le cycle cardiaque. Nous avons proposé une méthode basée sur une filtre de particules pour prédire le mouvement du cœur en tenant compte des paramètres géométriques et des valeurs d'intensité des cavités ventriculaires dans les images ETO. Nous avons constaté que la méthode était robuste aux frontières floues et aux informations manquantes. Nous pensons que l'automatisation du suivi du cœur est nécessaire dans la salle d'opération pour faciliter et estimer avec précision les informations de guidage dans la procédure hybride.

Mots-clés: les communications interventriculaires, échocardiographie, procédure hybride de fermeture des communications interventriculaires, fantômes cardiaques, système de mesure électromagnétique, guidage de navigation, simulation, cardiologie, cardiopathie congénitale, filtrage de particules, suivi du mouvement, imagerie diagnostique

Guidance in the Hybrid Cardiovascular Procedure for Ventricular Septal Defect Closure

Gerardo TIBAMOSO PEDRAZA

ABSTRACT

Ventricular septal defects (VSDs) are holes between ventricular cavities that disturb the normal blood oxygenation process. VSDs are common congenital heart malformations that usually close by themselves; however, large VSDs require surgical treatment. A hybrid procedure aims to implant occluders to close VSDs during beating heart, being less invasive than the most common open heart surgery. The procedure is monitored with transesopageal echocardiography (TEE). TEE supplies images at high frame rates in real time; nevertheless, TEE provides a limited field of view that hinders maneuvering of surgical instruments inside the heart. Therefore, high experience is required to interpret the TEE images and to maneuver the surgical instruments. However, medical simulators for training in the hybrid procedure are limited; hence, practicing directly on patients could remain as the only alternative.

The main goal of this thesis was to provide solutions to the problem of navigation guidance in the hybrid procedure to close VSDs. Those solutions are our three contributions that include: first, a method to design heart phantoms with VSDs for ultrasound imaging; second, a navigation guidance method to access VSDs for occluders implantation; and third, a cardiac motion tracking in ultrasound images of the heart with VSDs.

Our first contribution tackled the problem of a lack of heart models for experimentation. To solve this problem, we developed a method to built heart phantoms with VSDs for palpation, puncture, and ultrasound image acquisition. We relied on diagnostic images from retrospective cases to accurately represent the cardiac anatomy of pediatric patients with VSDs. We made heart phantoms in two materials: silicone and polyvinyl alcohol cryogel (PVA-C); we found that PVA-C had the best echogenicity, which was important for VSD characterization in echocardiography. We believe that this contribution provides additional tools to master the exploration of VSDs for the hybrid procedure.

Our second contribution tackled the problem of the limited field of view of TEE for guidance in the hybrid procedure. For the procedure's guidance, we introduced a three-dimensional (3-D) virtual model of the patient's heart and an electromagnetic measurement system (EMS) to track the surgical instruments. We validated a landmark registration method including heart phantoms, virtual heart models and the EMS in an experimental setup that we developed to simulate the hybrid procedure. A group of cardiologists performed the hybrid procedure on the heart phantoms, maneuvering the surgical instruments following the information provided by the virtual hearts. We found that the virtual heart models provided accurate information for guidance to access VSDs. We believe that this contribution is a successful proof of concept of a system that could provide guidance in a hybrid procedure, complementing TEE, to safely access VSDs.

Up to this point, we provide guidance information in a static heart. In a real case, however, the heart beats. Therefore, our third contribution tackled the problem to track the heart motion in ultrasound images with the potential application to synchronize the guidance information (second contribution) with the cardiac cycle. We proposed a method based on particle filtering to predict the heart motion considering geometric parameters and intensity values of the ventricular cavities in TEE images. We found that the method was robust to blurry boundaries and missing information. We believe that automation of the heart tracking can potentially facilitate guidance in the hybrid procedure.

Keywords: ventricular septal defects, echocardiography, hybrid procedure to close ventricular septal defects, heart phantoms, electromagnetic measurement system, navigation guidance, simulation, cardiology, congenital heart disease, particle filtering, motion tracking, diagnostic imaging

TABLE OF CONTENTS

Page

LIST OF TABLES

LIST OF FIGURES

LIST OF ABBREVIATIONS

2-D	Two Dimensions
3-D	Three Dimensions
6DOF	Six Degrees Of Freedom
AAM	Active Appearance Model
ASM	Active Shape Model
CMR	Cardiac Magnetic Resonance
CPB	Cardiopulmonary Bypass
CT	Computed Tomography
DC	Direct Current
DSC	Dice Similarity Coefficient
EMS	Electromagnetic Measurement System
GE	General Electric
ICP	Iterative Closest Point
LR	Landmark Registration
MRI	Magnetic Resonance Imaging
OR	Operation Room
PVA-C	PolyVinyl Alcohol Cryogel
RAM	Random Access Memory
RMS	Root Mean Square

TEE	Transesophageal Echocardiography
TTE	Transthoracic Echocardiography
US	Ultrasound
VSD	Ventricular Septal Defect
VSDs	Ventricular Septal Defects

INTRODUCTION

Ventricular septal defects (VSDs) are common heart malformations in newborns (Harold, 2014). A VSD is a hole in the wall that separates the left and right ventricular cavities. This abnormality could be problematic because in a normal heart, blood pressure and blood oxygenation in the two cavities are different; a hole between cavities alter the differences and could unbalance the circulatory system. Small VSDs do not represent a significant problem and usually they close by their own; conversely, large VSDs are considered causes of pulmonary overflow and heart failure (Dakkak & Oliver, 2021).

For newborns, open heart surgery is the prevalent procedure to close large VSDs. In this procedure, the heart is stopped and opened to suture patches in it to close the holes; a cardiopulmonary bypass (CPB) assumes the heart's functions while the heart is mended. Under certain conditions, however, a hybrid procedure to close large VSDs could be prescribed. In the hybrid procedure, occlusive devices are implanted through catheterization to close the holes during beating heart. The catheterization and device implantation are guided by means of transesophageal echocardiography (TEE).

0.1 Problem statement and motivation

TEE is the preferred imaging modality for the hybrid procedure to close VSDs. However, the limited field of view with TEE demands high experience maneuvering surgical instruments inside the beating heart to reach a VSD and implant an occluder device; avoiding any damage of sensitive tissues such as papillary muscles and valves. Indeed, complications during the hybrid procedure could imply intervention with more invasive techniques like the open heart surgery.

In search for complementary methods to support guidance for the hybrid procedure, we needed an experimental setup to recreate the conditions of a real case. The main component in the setup would be a physical model of a patient's heart with VSDs. The material properties of the model should allow palpation, puncture, and ultrasound image acquisition. Therefore, the research question in this stage of our project was: How to build a physical heart model that resembles anatomy, flexibility, and echogenicity of the heart of a pediatric patient with VSDs?

Pre-operative scans of the patient's heart are excellent sources of anatomical information. From them, surgeons and cardiologists analyse the patient's anatomy for intervention planning. We relied on those scans to define three-dimensional (3-D) virtual heart models that were used as an anatomical reference to build representations of a physical heart. The virtual models could also be used in the operation room (OR) to complement TEE for navigation guidance in the hybrid procedure. Therefore, we designed an experimental setup, which includes the virtual heart models, to conduct interventions of the hybrid procedure on the physical heart models (phantoms), looking for an answer to the question: How to use a patient-specific 3-D virtual heart model to support guidance in the hybrid procedure for VSD-closure?

In the experimental setup, the virtual and physical heart models were static. In a real case, however, the heart moves. Beating heart during the hybrid procedure could imply synchronization of additional information provided for guidance with the cardiac phase. On the other hand, we know that TEE provides excellent spatial and temporal information of a moving heart in real time. Therefore, our third research question was: How to track the heart motion in ultrasound images to identify the cardiac phase?

0.2 Research objectives and contributions

The main goal of our research project has been exploring alternatives to complement information provided by TEE for guidance during a hybrid procedure to close VSDs. With this goal in mind, we formulated three specific objectives to give answers to our research questions (Fig. 0.1). In this process, we faced multiple challenges and some failures; however, we reformulated our methods to overcome the difficulties. The final results are our three main contributions, which are described as follows.

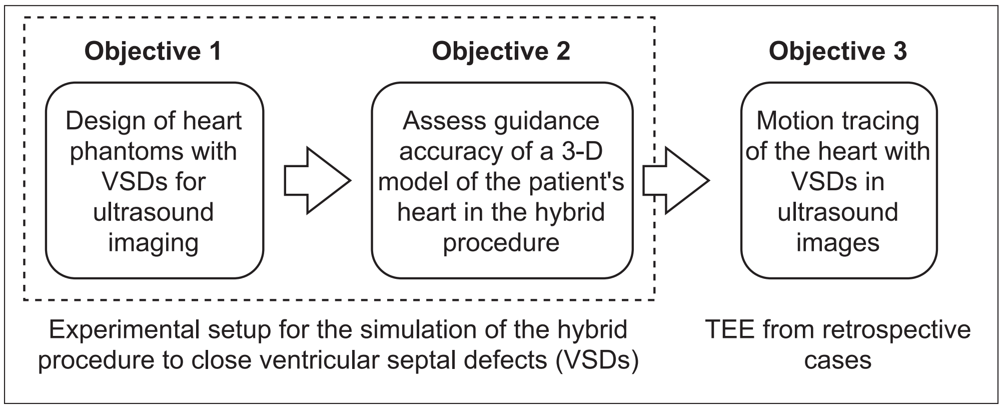

Figure 0.1 Research objectives to provide navigation guidance in the hybrid procedure to close ventricular septal defects (VSDs)

Our first contribution is a method to build physical heart models (heart phantoms) from pediatric patients with VSDs. Heart phantoms are valuable samples to experiment cardiac interventions. With our method, we built heart phantoms made of materials with appealing physical properties for a hybrid intervention; namely, the phantoms are soft-bodies with suitable echogenicity for VSDs characterization in ultrasound images. A detailed description of the proposed method and results are published by the International Journal of Computer Assisted Radiology and Surgery (IJCARS).

Our second contribution is an evaluation of a method to complement TEE information for guidance in the hybrid procedure. For this evaluation, we developed a experimental setup that includes heart phantoms (first contribution), where a group of cardiologists performed interventions to insert a needle and a guidewire inside the heart to access VSDs. We found that information provided by 3-D virtual heart models together with an electromagnetic measurement system (EMS) accurately contributes with the intervention guidance. A detailed description of the setup and the experimentation results are under review by the International Journal of Computer Assisted Radiology and Surgery (IJCARS).

Finally, our third contribution is a semi-automatic method to track heart motion on TEE images from patients with VSDs. Tracking heart motion provides information to identify the cardiac cycle, which is important for data synchronization in the navigation guidance method proposed in the second contribution, given that the hybrid procedure is performed during beating heart. We tackled the problem with particle filtering, which is a Bayesian method that combines a prior and a likelihood of the heart motion in ultrasound images to make predictions. Preliminary results were published in the international conference on image analysis and recognition (ICIAR 2017). We are writing a journal paper of this contribution for submission to Computer Methods and Programs in Biomedicine.

In summary, our scientific production includes (Appendix I):

- Contribution 1: One journal paper published in IJCARS, 2022 (Tibamoso-Pedraza *et al.*, 2022).
- Contribution 2: One journal paper under review by IJCARS, 2022.
- Contribution 3: One conference paper published in ICIAR 2017 (Tibamoso, Ratté & Duong, 2017), and one journal paper in preparation for submission to Computer Methods and Programs in Biomedicine, 2022.

0.3 Thesis Outline

This document is organized as follows. Chapter 1, literature review, comprises a description of the medical conditions and treatments of pediatric patients with VSDs; additionally, it provides a general description of methods to complement TEE in minimally invasive interventions for navigation guidance. Chapter 2 presents a detailed description of our first contribution, design of heart phantoms for ultrasound imaging of ventricular septal defects. Our second contribution, navigation guidance for ventricular septal defects closure in heart phantoms, is presented in Chapter 3. Chapter 4 presents our third contribution, Cardiac motion tracking in ultrasound imaging of ventricular septal defects. Finally, a general conclusion with recommendations for future work is provided.

CHAPTER 1

GENERAL LITERATURE REVIEW

1.1 Ventricular Septal Defects

In newborns, ventricular septal defects (VSDs) are highly common congenital heart malformations (Minette & Sahn, 2006; Penny & Vick, 2011; Dakkak & Oliver, 2021); however, their causes are not clearly known. VSDs are holes in the wall that separates the ventricular cavities, affecting normal blood circulation (Fig. 1.1 and Fig. 1.2). This condition could cause ventricular cavities enlargement and high blood pressure that could produce overload and premature wear of cardiovascular and lung tissues.

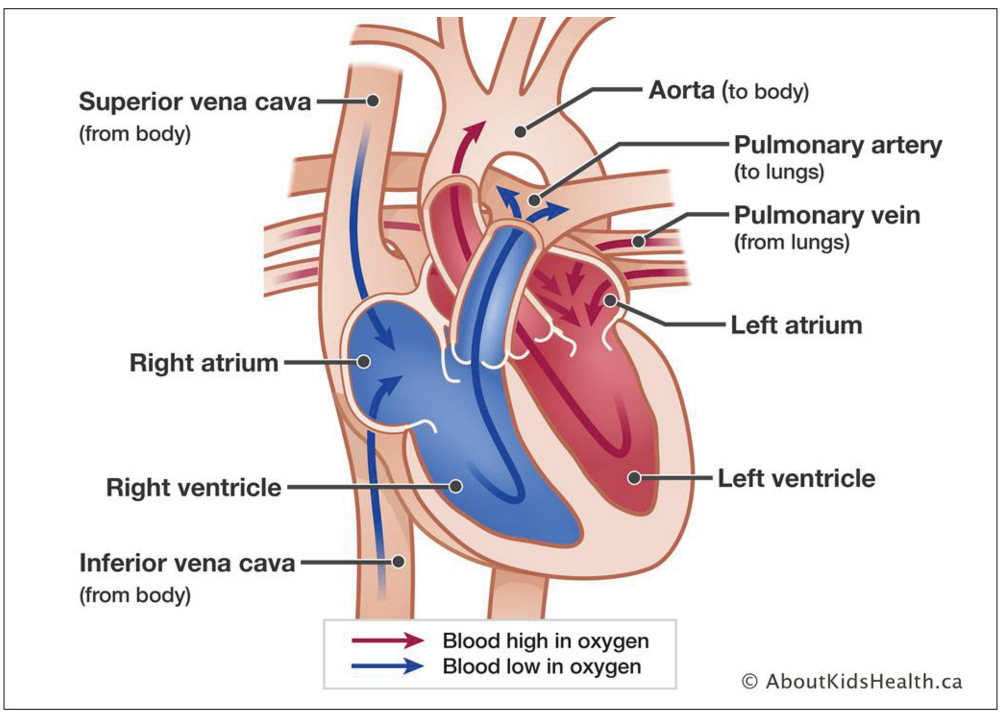

Figure 1.1 Graphical representation of normal blood circulation inside the heart. Image courtesy of the Hospital for Sick Children, www.aboutkidshealth.ca, ©2004-2021 AboutKidsHealth (SickKids staff, 2009)

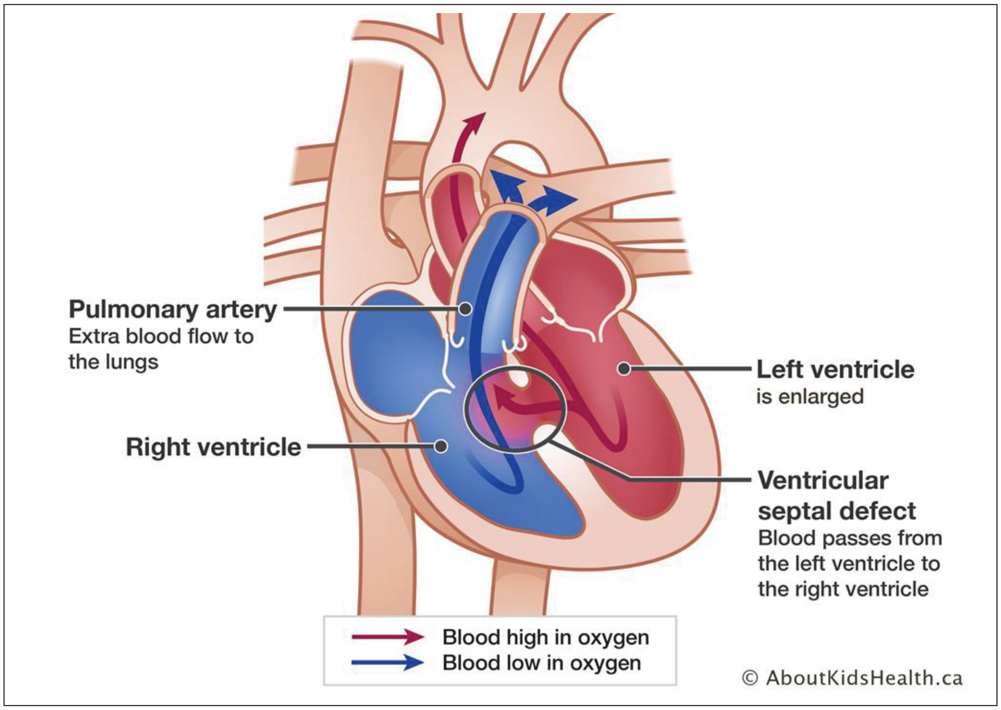

Figure 1.2 Graphical representation of an abnormal blood circulation inside the heart due to a ventricular septal defect. Image courtesy of the Hospital for Sick Children, www.aboutkidshealth.ca, ©2004-2021 AboutKidsHealth (SickKids staff, 2009)

1.2 Diagnosis and treatment of VSDs

Echocardiography provides images of the beating heart for detection and characterization of VSDs; sizes of VSDs are measured through echocardiography. Computed tomography (CT) and cardiac magnetic resonance (CMR) provide 3-D anatomical information of VSDs; from CT and CMR shape and location of VSDs could be identified for diagnosis and intervention planning. Small defects do not present major problems and they usually close by their own, but large ones could require surgical intervention (Penny & Vick, 2011).

In newborns, open heart surgery is a conventional procedure to close VSDs. In this procedure, the patient's heart is stopped and opened, and patches are stitched to close the holes; a cardiopulmonary bypass is required to take the heart's functions during the procedure (Penny & Vick, 2011). Minimally invasive techniques for VSDs closure have also been developed, but these can only be applied under certain clinical conditions. These techniques aim to implant occluder devices to close the VSDs during beating heart–a cardiopulmonary bypass is not required; the occluders are transported to the VSDs through thin tubes (catheters), which are inserted in the patient's body through small incisions. X-ray fluoroscopy is the preferred imaging modality to monitor and guide these minimally invasive interventions. Finally, a hybrid procedure to close VSDs is in between an open heart surgery and a minimally invasive technique (Amin, Berry, Foker, Rocchini & Bass, 1998; Li, Chen, Qiu, Lu & Wu, 2008; Xing *et al.*, 2010; Penny & Vick, 2011; Thakkar *et al.*, 2012; Haponiuk *et al.*, 2013; Sun, Zhu, Zhou, Guo & Zheng, 2016). The hybrid procedure is prescribed for small children when catheterization is not recommended, and location of VSDs are difficult to access with an open heart surgery. Transesophageal echocardiography (TEE) is the preferred imaging modality to monitor a hybrid procedure.

1.3 Hybrid procedure for VSD-closure

The hybrid procedure aims to implant a closure device in a VSD through a perventricular intervention during beating heart (Amin *et al.*, 1998; Yin, Zhu, Lin & An, 2014). In this procedure, the patient's heart is exposed after a median sternotomy, providing a direct access to the heart's surface (Fig. 1.3(a)). On the exposed region, the heart is punctured with a needle that conducts a guidewire to access the target VSD. When the guidewire reached the target, a catheter is inserted into the heart and through the VSD, following the guidewire's path. Then, an occluder device is inserted into the heart through the catheter and is implanted in the VSD (Fig. 1.4). TEE is the preferred and usually the only image modality to monitor every step of the hybrid procedure inside the beating heart (Fig. 1.3(b)).

1.3.1 Challenges during a hybrid procedure for VSD-closure

For a hybrid procedure, high experience is required to maneuver the TEE probe and to interpret the acquired TEE images. When the TEE probe is inserted in the patient's esophagus, the TEE images are the main information to select the position and orientation of the probe to monitor a VSD (Fig. 1.5). Maneuvering a TEE probe is difficult; improper movements of the TEE probe

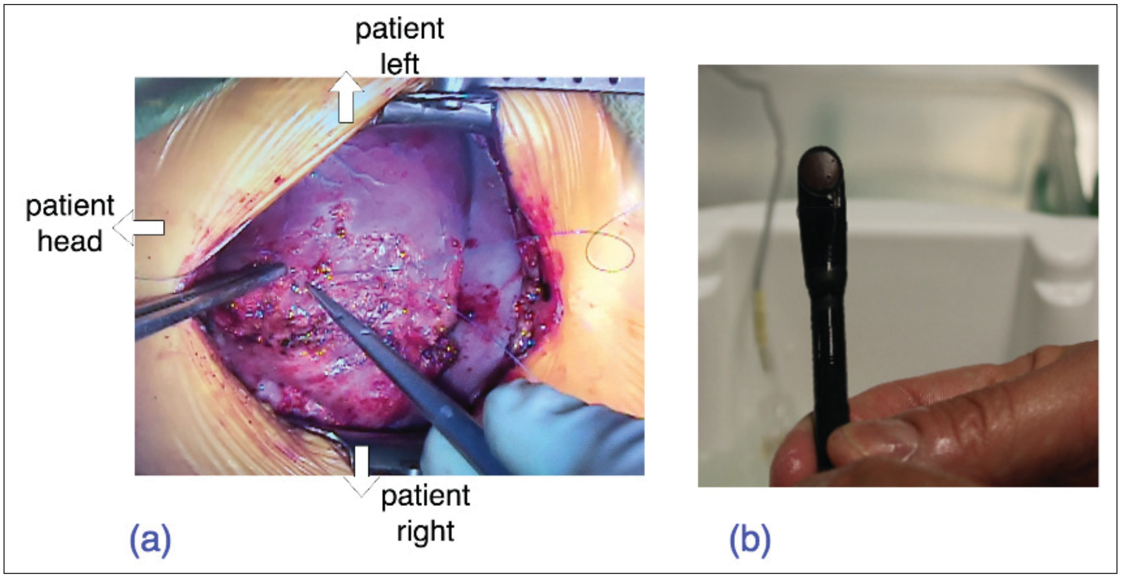

Figure 1.3 Hybrid procedure to close ventricular septal defects (VSDs). (a) Exposure of the patient's heart; (b) transesophageal echocardiography (TEE) probe for intervention guidance

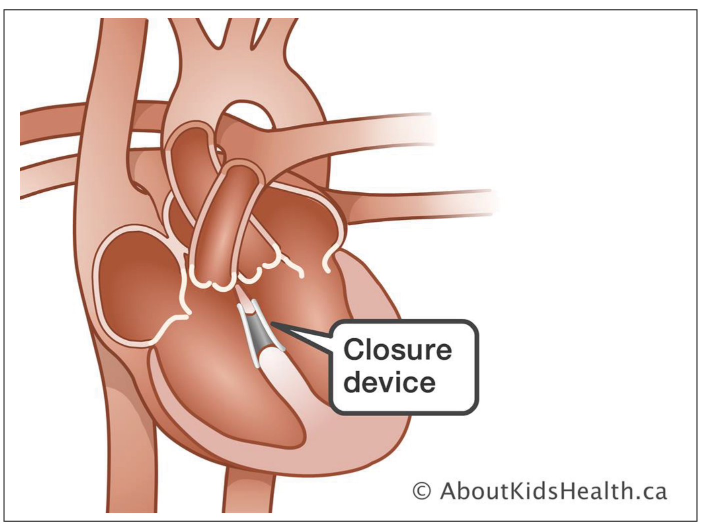

Figure 1.4 Occluder device implanted closing a VSD. Image courtesy of the Hospital for Sick Children, www.aboutkidshealth.ca, ©2004-2021 AboutKidsHealth (SickKids staff, 2009)

could tear the sensitive patient's esophagus. Additionally, slight rotations or slight translations of the TEE probe greatly change the anatomical information of the acquired TEE images. A clear understanding of the TEE images could facilitate the heart puncture, catheter insertion, and occluder device implantation, to close a VSD without piercing susceptible cardiac tissues such as papillary muscles and valves (Crossland *et al.*, 2008). The complexity is even greater because the procedure is performed during beating heart, which means that the target VSD is in a continuous motion. For complex cases, however, TEE may not be enough for intervention guidance; the limited field of view of TEE could hinder monitoring of surgical instruments inside the heart to close a VSD. Complications in the hybrid procedure could imply several heart punctures, or the intervention with an open heart surgery (Crossland *et al.*, 2008; Thakkar *et al.*, 2012).

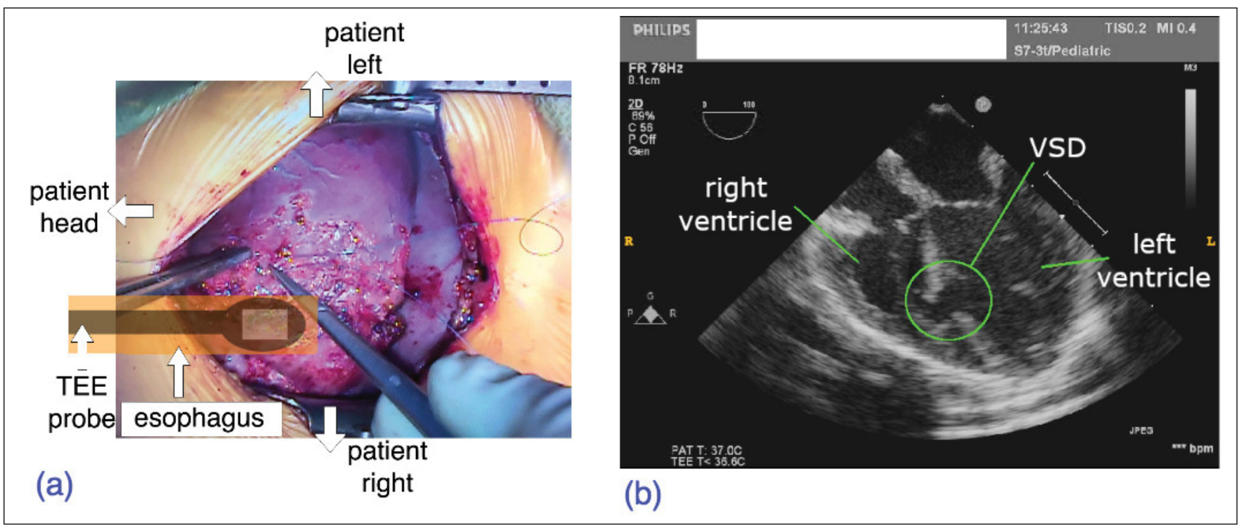

Figure 1.5 Image acquisition during a hybrid procedure to close a ventricular septal defect (VSD). (a) Representation of a transesophageal echocardiography (TEE) probe inserted in the patient's esophagus; (b) TEE images of a patient with a VSD in a four chamber view

1.3.2 Alternatives to provide guidance in a hybrid procedure for VSD-closure

Intervention planning of a hybrid procedure to close a VSD include identification of anatomical landmarks such as the atrio-ventricular valves, papillary muscles, and the target VSD. Palpation of the patient's heart is a common practice to facilitate landmarks identification under the support of TEE imaging. With the collected information, a puncture site is selected for a perventricular access through the right ventricle free wall (in some cases, however, the puncture is performed on the right atrium free wall). When a needle punctures the heart, the needle should be headed for the target VSD; the complexity of the procedure in this stage is to visualize the target VSD and the inserted needle, simultaneously, in the same TEE image plane. Therefore, introducing measurement instruments or additional image modalities could provide additional information for guidance during this critical stage of the procedure.

Complementing TEE with X-ray fluoroscopy could be an alternative to facilitate monitoring and guidance of the hybrid procedure, as it has been explored for minimally invasive interventions (Lang *et al.*, 2012; Biaggi, Fernandez-Golfín, Hahn & Corti, 2015; Jone *et al.*, 2016; Thaden *et al.*, 2016). Basically, images from the two modalities are related via an automatic pose detection and tracking of the TEE probe–inside the patient's esophagus–through the X-ray images. Knowing position and orientation of the TEE probe facilitates the estimation of the TEE field of view and the interpretation of the TEE images. Validation accuracy of this method has shown promising results, and the procedures have required minimum X-ray dose radiation. However, training and specialized equipment are required, and the system works with a 3-D TEE probe, which is bigger than the conventional 2-D TEE probe used in the hybrid procedure, prohibiting its use in newborns (Jone *et al.*, 2016).

Instead of X-ray fluoroscopy, position and orientation of the TEE probe could be measured with an electromagnetic measurement system (EMS) (Linte *et al.*, 2009; Luo, Cai & Gu, 2013; Moore *et al.*, 2013; McLeod *et al.*, 2016). For minimally invasive interventions, an EMS is probably the most suitable tool to record information from surgical instruments that are inside the patient's body and therefore not in line of sight. Information provided by an EMS could be used to represent the surgical instruments in a virtual environment, together with anatomical representations of the patient's heart extracted from preoperative scans (CT or CMR). This strategy has shown benefits for image interpretation and catheter guidance (Luo *et al.*, 2013; Moore *et al.*, 2013; McLeod *et al.*, 2016). However, its validation in clinical practice is still a challenge due to the intrinsic heart dynamic behaviour, sterilization protocols, system calibration, and electromagnetic interference due to ferromagnetic materials in the operation room (Linte *et al.*, 2013; Franz *et al.*, 2014).

Finally, three-dimensional echocardiography has a potential application in the hybrid procedure, because it could provide spatial and temporal information that could facilitate recognition of surgical instruments and cardiac structures of interest in a 3-D anatomical context (Balzer *et al.*, 2008; Marx, 2014; Faletra *et al.*, 2014). However, technological improvements for 3-D TEE are required to reach 2-D TEE spatial and temporal resolutions, and additionally a size reduction of the 3-D TEE probe to be used in pediatric patients.

1.4 Discussion

Transesophageal echocardiography (TEE) is a fundamental tool for guidance in the hybrid procedure to close ventricular septal defects (VSDs). TEE, however, provides images with a very limited field of view, which hinders maneuvering surgical instruments inside the beating heart to access a target VSD.

Introducing X-ray fluoroscopy to complement TEE in the hybrid procedure is not convenient; X-ray should be avoided in this procedure because a team of surgeons and cardiologists are in close proximity to the patient. It is known that exposure to X-ray could produce short- and long-term damage of biological tissues.

An electromagnetic measurement system (EMS) could be appropriate to complement information provided by TEE in the hybrid procedure. Optical tracking is also an appealing alternative to provide spatial information to guide punctures in the procedure. However, both EMS and optical tracking should be robust and accurate enough under working conditions in the operation room.

A three-dimensional model of a patient's heart could provide valuable anatomical information of VSDs for the hybrid procedure. Pre-operative scans from computed tomography (CT) or cardiac magnetic resonance (CMR) are appealing sources of accurate information for the model's design. Displaying the heart model of the patient's heart in the operation room would facilitate intervention planning; adding an EMS or an optical tracking would facilitate navigation guidance.

Emerging technologies in virtual and augmented reality could be translated in the operating room to support surgical interventions. Those technologies already support training and planning of interventions; however, feasibility, cost, and accuracy are some of the main concerns related to the integration of these technologies in the operation room.

This chapter provided a clinical context of our research problem and cited relevant works to gain insight of the challenges and opportunities to explore innovative solutions in the hybrid procedure for VSD-closure. The next three chapters present three specific problems related to the hybrid procedure; each of these chapters begins exploring related works that provided insight and inspiration for our contributions.

CHAPTER 2

DESIGN OF HEART PHANTOMS FOR ULTRASOUND IMAGING OF VENTRICULAR SEPTAL DEFECTS

2.1 Introduction

Ventricular septal defects (VSDs) are common congenital heart malformations in newborns. VSDs leave holes in the ventricular septum that could cause pulmonary overflow and heart failure (Dakkak & Oliver, 2021). Complex VSDs are treated using a hybrid procedure, combining both cardiac surgery and cardiac catheterization, recommended when an open heart surgery is less feasible. The hybrid procedure is underpinned by echocardiography to guide an implant device to close the holes during beating heart (Amin *et al.*, 1998).

The severity of VSDs depends on the size, shape, and location of the holes; characteristics generally identified by means of echocardiography (Dakkak & Oliver, 2021). Echocardiography is a complex image modality; hence, extensive training is required for an appropriate image acquisition and interpretation. Training with heart simulators could complement learning of echocardiography during hybrid procedures (Harrison & Gosai, 2017); however, the cost and complexity of the simulators could hinder the possibility to include patient-specific heart models with complex VSDs.

Rapid prototyping allows to build patient-specific heart models with complex VSDs (Bhatla *et al.*, 2017); however, commercial materials for three-dimensional (3-D) printing, such as plastics and resins, are still not appropriate for ultrasound imaging. To overcome this limitation, casting has been used, which requires molds to reproduce heart models (phantoms) in a broader spectrum of materials. Indeed, water-based (polyvinyl alcohol cryogel [PVA-C]) and no water-based (silicone and ballistic gel) materials have been tested using casting (Morais *et al.*, 2017; Laing *et al.*, 2018; Alves *et al.*, 2020).

Morais *et al.* (2017) proposed a method to build heart phantoms to represent the atriums and the inter-atrial septum. Laing *et al.* (2018) proposed a method to build heart phantoms to represent an extensive atrioventricular region including the mitral valve. Alves *et al.* (2020) proposed a method to build phantoms of the whole heart (atriums and ventricles) with the interest to evaluate its acoustic properties. For casting, Morais *et al.* (2017) and Laing *et al.* (2018) tested silicone and PVA-C, and Alves *et al.* (2020) tested ballistic gel. Morais *et al.* (2017) found similar behavior from both materials when they were scanned with ultrasound. Morais *et al.* (2017) and Laing *et al.* (2018) found that silicone has advantages over PVA-C considering processing complexities, production times, and preservation requirements. However, an appealing quality of PVA-C is its potential capacity to resemble mechanical properties of biological tissues given its high water content (Morais *et al.*, 2017; Wan, Campbell, Zhang, Hui & Boughner, 2002; Surry, Austin, Fenster & Peters, 2004). Alves *et al.* (2020) found a recipe with ballistic gel to mimic acoustic properties of biological tissues. Finally, from the ultrasound images reported by Morais *et al.* (2017), Laing *et al.* (2018), and Alves *et al.* (2020) we observed similar attenuation patterns of the models made of silicone and ballistic gel.

The main goal of this study is to build heart phantoms of newborns with complex VSDs. The specific goals are to validate with two different materials (silicone and PVA-C), to evaluate measurements of the VSDs, and finally, to provide valuable insights on the design of heart phantoms for ultrasound imaging of VSDs.

2.2 Materials and Methods

From preoperative scans–computed tomography (CT) or cardiac magnetic resonance (CMR)–we designed heart phantoms of newborns with VSDs. The method is divided in three main steps: image segmentation, molding, and casting. For validation, we acquired 2-D ultrasound images from three heart phantoms, reconstructed a volume representation, and evaluated ventricular shapes and sizes of VSDs.

2.2.1 Dataset

Three retrospective cases of newborns with complex VSDs were collected from Sainte-Justine Hospital. The data included two CT and one CMR preoperative scans, with image resolution of 0.23 x 0.23 x 0.4 mm^3, 0.27 x 0.27 x 1.25 mm^3, and 0.63 x 0.63 x 5 mm^3, respectively. Before image segmentation, we redefined image's resolution of cases two and three to 0.27 x 0.27 x 0.27 mm^3, and 0.63 x 0.63 x 0.63 mm^3, respectively, using cubic interpolation. This step allowed us to segment regions with more detail and obtain smooth boundaries.

2.2.2 Cardiac Image Segmentation

We manually segmented images from the scans–guided by a cardiologist–to shape a 3-D region that includes left and right atriums, left and right ventricles, pulmonary artery, and aorta and filling spaces between them to obtain a solid body of the whole heart. From this region, we extracted boundaries of 3 mm thickness, and afterwards we segmented the septum's region to define the ventricular and atrial cavities. Then, we divided the remaining structure in two parts (atriums and ventricles), and added rims in their boundaries to facilitate their assembly after casting (Fig. 2.1). Finally, the segmented regions were modeled as polygonal meshes. For all these operations we used 3D Slicer (www.slicer.org), which facilitates navigation in the 3-D data and the use of binary operations to refine and smooth the segmented regions.

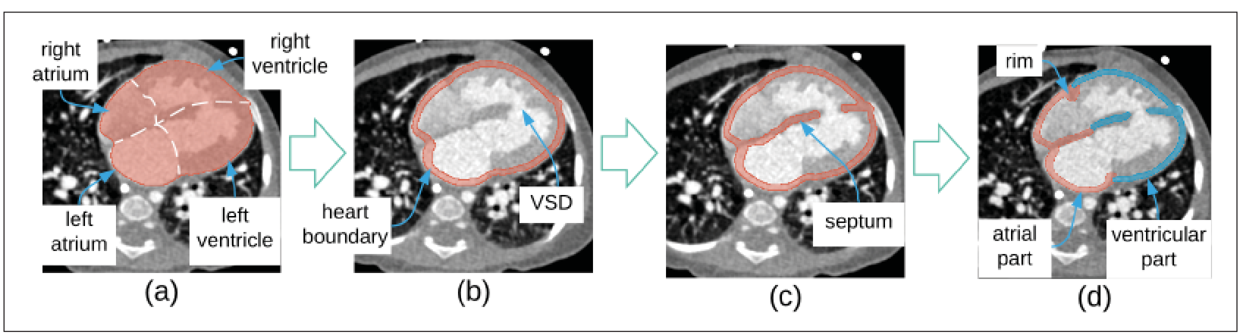

Figure 2.1 Cardiac image segmentation. (a) Whole heart segmentation, (b) heart boundaries' extraction, (c) septum demarcation, and (d) separation of atrial and ventricular parts

The polygonal meshes, which represent the whole heart (atriums and ventricles), were refined using Meshlab. Basic boundary-preserving decimation and smoothing filters were applied to reduce the number of polygons while preserving anatomical details. To this end, for each model we applied the filter Quadric Edge Collapse Decimation several times, until the number of polygons were around 30.000. To highly preserve the original model's shape and size, the parameters of the decimation filter were defined as follows: percentage reduction: 0, quality threshold: 1.0, boundary preserving weight: 1, preserve boundary of the mesh: on, preserve normal: on, preserve topology: on, optimal position of simplified vertices: on, planar simplification: on, weighted simplification: off, post-simplification cleaning: on, and simplify only selected faces: off. Thereafter, the filter HC Laplacian Smooth was applied once, and the resultant model was saved in stl format. These were the reference models for molds design (casting), and also the gold standard to compare with the reconstructed models from the heart phantoms in the validation step.

2.2.3 Molding and Casting Heart Phantoms

We designed molds to reproduce the two parts of each heart phantom in two different materials: PVA-C and silicone. Afterwards, the parts were assembled to shape whole heart phantoms (Fig. 2.2).

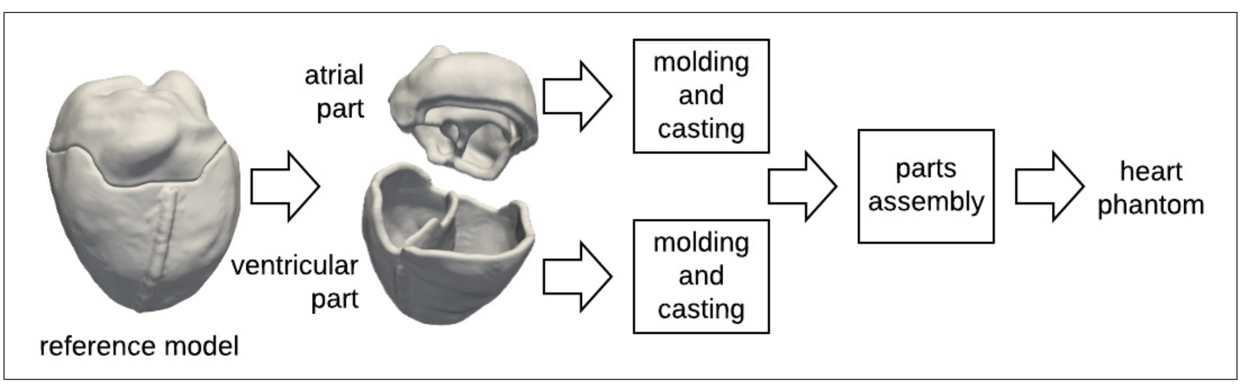

Figure 2.2 Steps to build a heart phantom. Atrial and ventricular parts are reproduced individually, and they are assembled to shape a whole heart phantom

2.2.3.1 Molding

The initial mold design was obtained by computing the Boolean difference between a solid block and each part of the models. We chose a cylindrical shape for the solid block, which is divided in two pieces for unmolding purposes. Then, two holes were added to the mold: one that connects with deep regions to pour the silicone or PVA-C for a bottom-up filling; the other connects with the regions at the top to allow the exit of air bubbles. Additional partitions to the mold were made to facilitate unmolding after casting. The mold's pieces were aligned with pin-hole pairs made in corresponding faces (Fig. 2.3). We used Autodesk Meshmixer for the mold design (www.meshmixer.com).

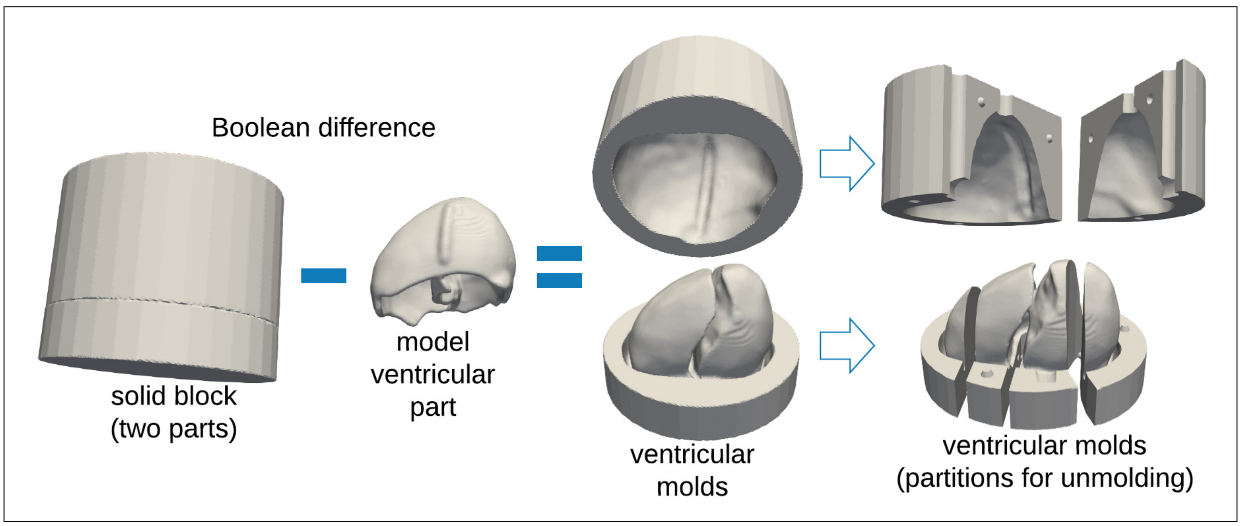

Figure 2.3 Molds design. Boolean difference is the main operation, followed by partition of the molds to facilitate the unmolding after casting

The mold's pieces were printed in 3-D with thermoplastic polymer (Materio3D PLA 3D850 1.75mm) by an Original Prusa i3 MKS (Prusa Research, Prague, Czech Republic) with the following settings: quality=0.15 mm, infill=15%, support=none, and brim=off. The printed pieces were assembled and tied with plastic bands, and fissures between them were filled with a fine layer of commercial silicone to avoid leaking. However, before the assembly, we spread a fine layer of petroleum jelly (petrolatum 100%) to the opposite faces of the pieces that shape the

VSDs, which aimed to inhibit the cure of silicone or restrain the access of PVA-C in that region and assure the holes in the phantoms.

2.2.3.2 Casting with Silicone

We chose Smooth-On Ecoflex 00-30 (Smooth-On, PA, USA), platinum catalyzed silicone, which has shown good results modeling atrial cavities for ultrasound imaging (Laing *et al.*, 2018). We followed the manufacturer's instructions to prepare the silicone, namely mixing components A and B (equal proportions), and degassing the mix in a vacuum chamber (-30 inHg). We noticed that the time for mixing and degassing is short (5 min approx.), because the viscosity of the silicone increases quickly. Also for this reason, we prepared silicone for each mold individually. Immediately after its degassing, the silicone was poured into the molds and let to rest in it for 12 hours at room temperature before unmolding. After unmolding, the two parts of the phantom were assembled and glued together with a fine layer of a new preparation of the same silicone, and left them to rest for 12 more hours. For the assembly, the two parts were supported on the external section of the ventricular mold.

2.2.3.3 Casting with PVA-C

PVA hydrogel, which is the base for the PVA-C, was produced mixing PVA and distilled water in a proportion of 15 % and 85 % by weight, respectively. The PVA's properties that we used include 98-98.8 % hydrolyzed and M.W. approx. 50.000-85.000 (ACROS ORGANICS, Thermo Fisher Scientific, MA, USA, code: 183381000). The components were constantly mixed in an Erlenmeyer flask with a magnetic stir bar (180 rpm), over a heater plate that kept the mix at 80-90 °C, until the PVA was dissolved (2-3 h approx.). The level of the mix was supervised during all the mixing time, and distilled water was added when required. Thereafter, the resultant hydrogel was left at rest for 6h to reach room temperature and to release any remaining air bubbles.

Then, the PVA hydrogel was poured into the molds, let to rest for a couple of hours (allowing the exit of air bubbles), and exposed to three freeze-thaw cycles to form the PVA Cryogel (PVA-C).

We used a commercial freezer, but we instrumented it to control the change of temperatures in a stair-wise manner. The instrumentation included a temperature sensor inside the freezer, a relay in one of the lines of the freezer power connector, and a Raspberry Pi that received the sensor information and controlled the relay.

Each freeze-thaw cycle began from room temperature (20 °C approx.) to -20 °C, with a freezing rate of -0.2 °C/min on average. Then, the temperature was held on -20 ± 2 °C for 6 h (control on-off between -18 and -22 °C). Afterwards, the temperature increased from -20 °C to 20 °C with a thawing rate of 0.06 °C/min on average; low thawing rate benefits the PVA-C formation (Wan *et al.*, 2002). After the three cycles, we unmolded and assembled the two parts that shape each heart phantom–using the external parts of the ventricular molds as support. In order to glue the parts firmly, three additional freeze-thaw cycles were required (cycles with same properties as before), spreading a layer of the PVA hydrogel in the junctures just before the beginning of each cycle.

2.2.4 Validation

We acquired ultrasound (US) images from the heart phantoms to evaluate the shape of ventricular cavities and sizes of VSDs. To do this, we reconstructed 3-D models of the phantoms from their images. These models were compared with the respective models of reference. We used Dice similarity coefficient (DSC) to measure shape similarity between them, and estimated areas and diameters of VSDs.

The models' reconstruction involved 3-D reconstruction of the ultrasound images. For the latter, we recorded the position and orientation of the US probe together with the respective US images–sweeping the ventricular region of the phantom that was full of and immersed in water. The volume reconstruction algorithm included in the PLUS toolkit library (Lasso *et al.*, 2014) was used to reconstruct a data volume of 0.5 x 0.5 x 0.5 mm^3 resolution. Then, we manually segmented the images of this volume for the reconstruction of each model.

The ultrasound images were acquired with a TOSHIBA PLT-704AT 7.5 MHz Linear array transducer (US probe), and the probe position and orientation were tracked with an electromagnetic measurement system (EMS) (Aurora V2, NDI, Canada) (Fig. 2.4). We used the Freehand tracked ultrasound calibration application (fCal) to estimate the image to tracker transform; using the spatial and the temporal calibrations of fCal, we achieved accuracy errors less than 0.70 mm RMS.

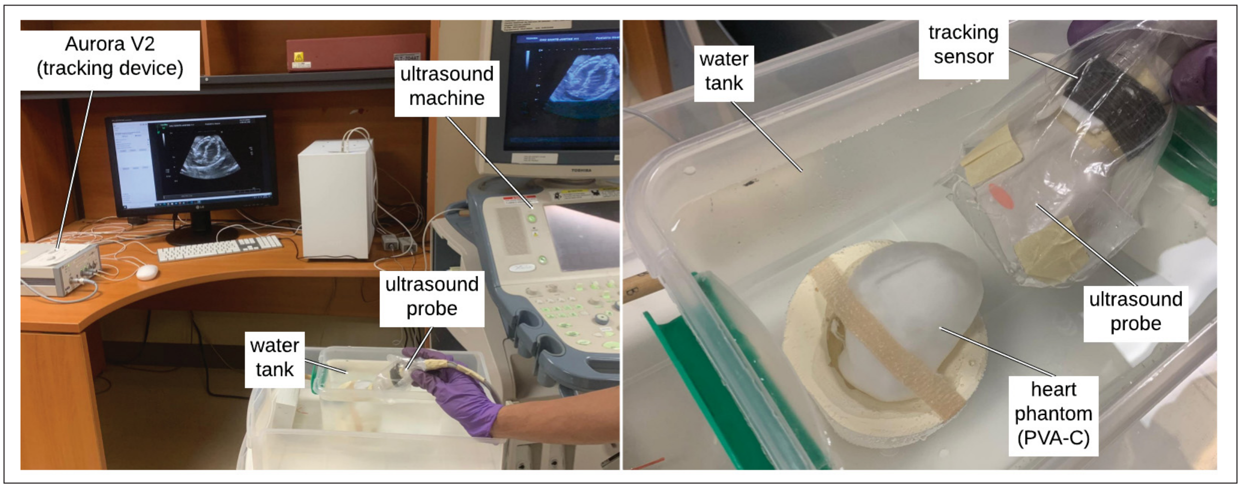

Figure 2.4 3-D ultrasound reconstruction. (Left) Setup that includes ultrasound machine, electromagnetic tracking device (Aurora V2), desktop computer, and a water tank. (Right) A heart phantom in the water tank for ultrasound image acquisition

Afterwards, the respective reconstructed and reference models were aligned by rigid transformations in two steps. The first step transformed one model towards the other aligning four corresponding points, which were defined manually over the two surfaces. The second step automatically refined the alignment of the models by an Iterative Closest Point algorithm (ICP, implemented in the Visualization Toolkit [www.vtk.org]). Finally, the models were transformed into image segmentation, and DSC was calculated. The tools for alignment and DSC calculation were found in 3D Slicer (slicerIGT and SegmentRegistration extensions).

On the other hand, sizes of the VSDs were estimated by hand, covering the area of the holes in the 3-D space with triangular segments. For each hole, all triangular segments had a common vertex, which was defined at the middle of the hole, and the other vertices were regularly spaced along the hole's boundaries. From these partitions, area and size (diameters) of a VSD were estimated. The area was estimated adding up the areas of all the triangular segments; the diameters, adding up the magnitude of each pair of triangle's edges that touch the common vertex and are 180 degrees apart, obtaining a list of values from where we calculated maximum, minimum, mean, and standard deviation.

2.3 Results

Four large VSDs were identified and represented accordingly in the reference heart models from the three retrospective cases (Fig. 2.5). VSDs diameters were between 4.8 mm and 8.8 mm (Table 2.1). Dimensions of the one, two, and three heart models were 80 x 65 x 55 mm^3, 70 x 60 x 45 mm^3, and 80 x 60 x 50 mm^3, respectively. Some images of the casting process are presented in Fig. 2.6. The reusable molds allowed us to reproduce similar phantoms made of silicone or PVA-C. Less than 100 ml of the silicone or PVA hydrogel was required to build a whole heart phantom.

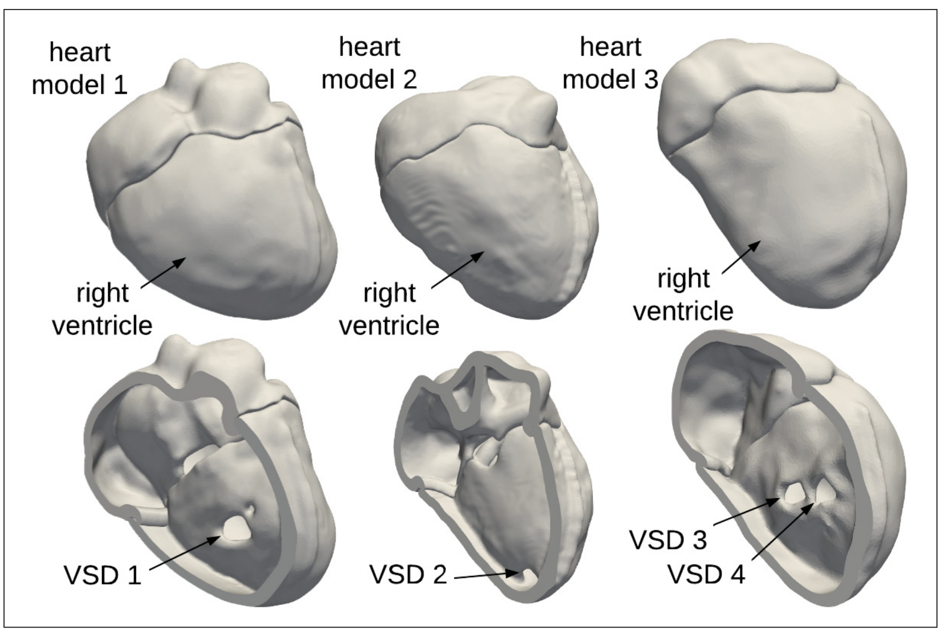

Figure 2.5 Reference heart models. Upper row shows the assembled heart models; lower row shows the ventricular septums and VSDs of the models

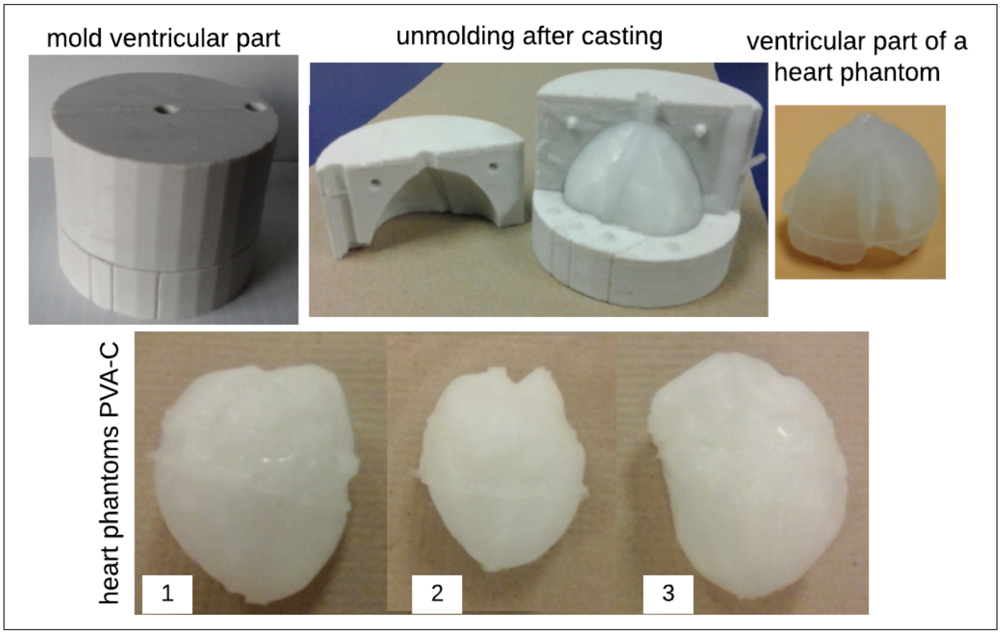

Figure 2.6 Casting a heart phantom. Images of a mold, unmolding, and the final results to make heart phantoms

2.3.1 Validation

We acquired ultrasound images from the phantoms made of silicone and also from those of PVA-C (Fig. 2.7). Boundaries of VSDs of the models made of silicone were not clear enough for image segmentation. In contrast, we observed better definition of VSDs in the images of the phantoms made of PVA-C. Hence, only reconstructions of the phantoms made of PVA-C were obtained; therefore, the following measurements are related to them.

Fig. 2.8 compares reference and reconstructed phantoms, where we can see shape similarities between ventricular regions. The DSC for each of the three heart phantoms was evaluated respectively at 0.71, 0.76, and 0.64. We estimated diameters and areas of the four large VSDs in the reference and reconstructed models of the three heart phantoms (Table 2.1 and Table 2.2). For all four VSDs, absolute value of errors in minimum (min.) and mean diameters were lower than 1 mm, and not more than 1.1 mm for the maximum (max.) diameters. Error in the areas were lower than 15%, with the exception of VSD 3 whose error was 24% (7.4 mm^2).

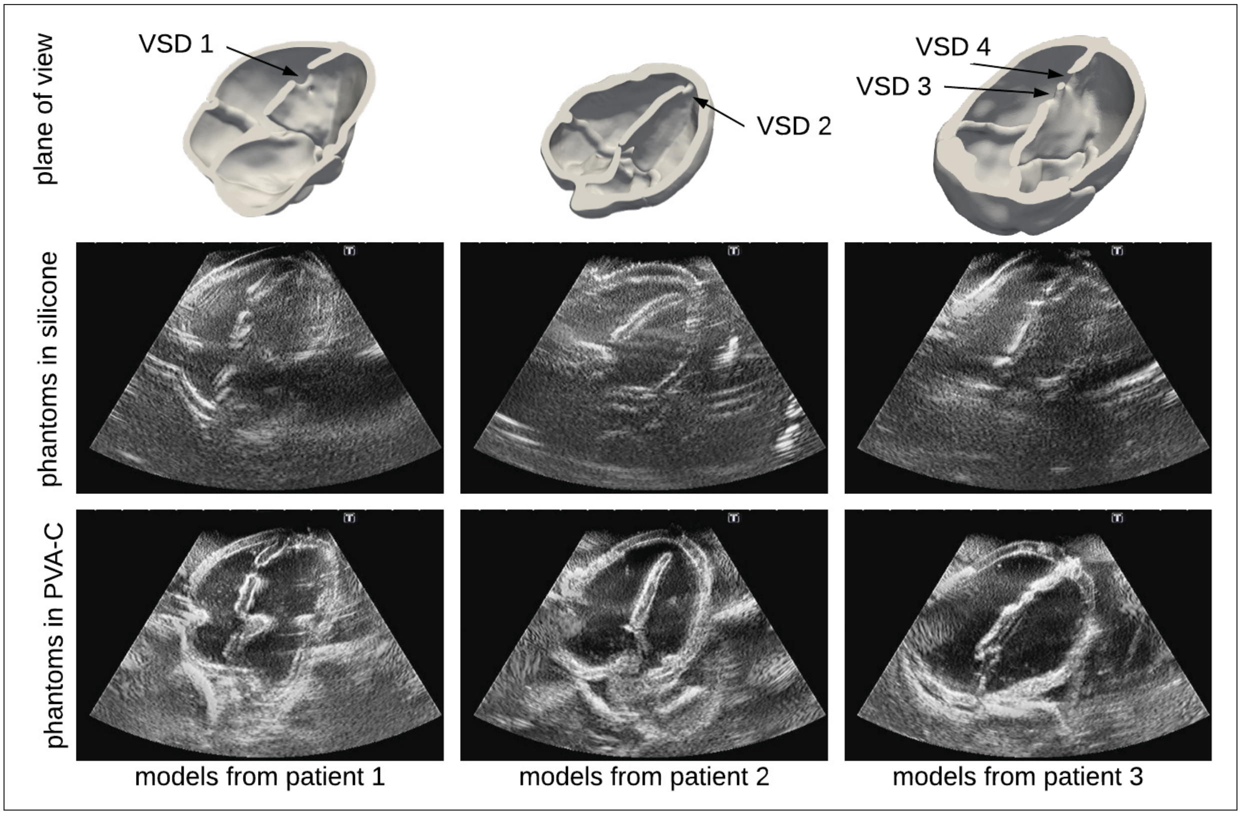

Figure 2.7 Visualization of VSDs in ultrasound images acquired from the heart phantoms made of silicone and PVA-C

Generally, VSDs in the reconstructed models were smaller than those in the reference ones, with the exception of VSD 4 that was slightly oversized.

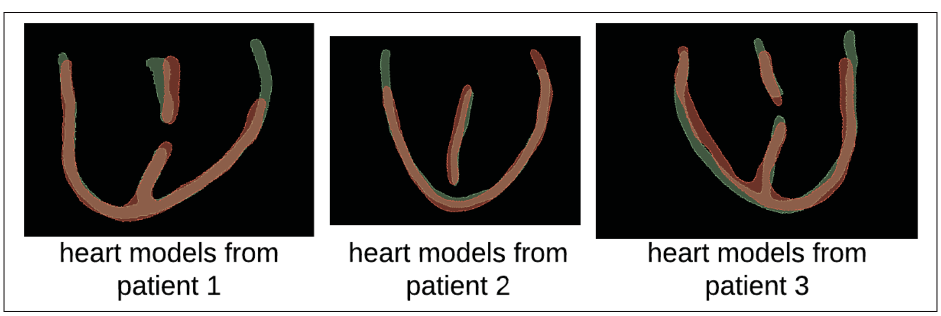

Figure 2.8 Image of the comparison between reconstructed (red) and reference (green) models for the heart phantoms made of PVA-C

Table 2.1 Measurements of areas and diameters (maximum, minimum, mean and standard deviation) of the four ventricular septal defects (VSDs) from the reference (ref.) and reconstructed (rec.) models of the three heart phantoms made of PVA-C

heart models		VSD	area (mm^2)	diameter (mm) max.	min.	mean	std.
1	ref.	1	44.4	8.8	6.1	7.5	0.9
1	rec.	1	38.1	8.5	5.7	6.9	1.0
2	ref.	2	32.4	8.0	5.0	6.4	1.0
2	rec.	2	32.3	6.9	5.9	6.4	0.3
3	ref.	3	30.9	7.4	4.8	6.2	0.9
3	rec.	3	23.5	6.4	4.4	5.4	0.7
3	ref.	4	31.8	7.0	5.1	6.3	0.6
3	rec.	4	35.1	7.7	5.4	6.6	0.7

Table 2.2 Error estimation of the measurements of areas and diameters (maximum, minimum, mean and standard deviation) of the four ventricular septal defects (VSDs) from the reference (ref.) and reconstructed (rec.) models of the three heart phantoms made of PVA-C

heart model	VSD	area error (mm^2)	(%)	diameter max. error (mm)	(%)	min. error (mm)	(%)	mean error (mm)	(%)
1	1	-6.3	-14.2	-0.3	-3.4	-0.4	-6.6	-0.6	-8.0
2	2	-0.1	-0.3	-1.1	-13.8	0.9	18.0	0.0	0.0
3	3	-7.4	-24.0	-1.0	-13.5	-0.4	-8.3	-0.8	-12.9
3	4	3.3	10.4	0.7	10.0	0.3	5.9	0.3	4.8

2.4 Discussion

We developed a method to build whole heart phantoms of newborns for ultrasound imaging of complex VSDs. We found that ultrasound images acquired from three heart phantoms made of PVA-C shown better definition of their VSDs than the images acquired from the respective phantoms made of silicone. Image quality from the phantoms made of PVA-C facilitated VSDs size characterization. These results suggest that water-based materials, such as PVA-C, could mimic better tissue echogenicity of cardiac structures than no water-based ones (silicone).

We found good accuracy in sizes of VSDs and shapes of ventricular cavities of the heart phantoms made of PVA-C. However, multiple factors may have contributed with errors in these representations. One of these factors is that each freeze-thaw cycle dehydrated the phantoms making them slightly thinner. Other is the approximations made during acquisition, reconstruction, and segmentation of the ultrasound images. Another factor is that casting and parts assembly involves manual skills. Improvements of these factors, including fewer freeze-thaw cycles, 3-D scans of the phantoms with computed tomography or magnetic resonance imaging, and casting the whole heart as only one piece, could reduce those errors in accuracy.

Our method allows to build whole heart phantoms as an assembly of two parts. Assembling the parts in silicone was straightforward, but assembling those in PVA-C depended on the material density. Empirically, we found that at least 15% of PVA (by weight) in the hydrogel produces parts rigid enough for successful assembling; lower than that the material consistency hinders the parts merging.

From our experience, we observed that tiny air bubbles attach to the surfaces of the silicone and the PVA-C heart phantoms when they are immersed in water. Removing manually these air bubbles–required for appropriate ultrasound imaging–was more difficult from the phantoms in silicone than those in PVA-C. Perhaps this behavior is due to the impermeability and electrostatic properties of the silicone that could keep attached harder the bubbles, which differ from wet materials like PVA-C.

Image segmentation of complex VSDs is very challenging due to the anatomical complexity and limitations in image quality, image resolution, and contrast. Indeed, muscular and membranous fibers interconnected the septum, ventricular walls, and the atrioventricular valves, which misled the definition of VSDs, especially when edges of the defects were misaligned. Therefore, we manually segmented the images under the supervision of a cardiologist. This time-consuming task can take up to 8 hours, which outlines the need for further development of fully automatic segmentation methods (Decourt & Duong, 2020).

Rapid prototyping methods are evolving very fast and future advances could boost strategies to build phantoms more efficiently. The time to make a full heart phantom with complex VSDs was evaluated between 6 and 10 days: a day for image segmentation; a day for molds design; one to two days for 3-D printing; two and six days for casting in silicone and PVA-C. This process could be optimized with experience.

We estimated the cost of one heart phantom at $500 USD (in currency of 2021), which includes: $25 materials, $125 renting of machinery, and $350 labor. However, an additional copy of the same heart could cost less than $100 because the molds are reusable. A greater scale production could reduce the materials and machinery costs, but a substantial cost reduction in labor could be achieved by improving the segmentation strategy, namely introducing automatic or semi-automatic segmentation methods to speed up the manual process.

Future work will focus on investigating new approaches to fully automate the segmentation and the identification of VSDs on preoperative imaging.

2.5 Conclusion

Rapid prototyping allowed us to formulate and test an approach to build heart phantoms for ultrasound imaging of VSDs. Results suggest that ultrasound images from phantoms made of PVA-C allow VSDs size characterization with good accuracy. Future work includes evaluation of the heart phantoms during the simulation of hybrid procedures for closure of complex VSDs.

CHAPTER 3

NAVIGATION GUIDANCE FOR VENTRICULAR SEPTAL DEFECTS CLOSURE IN HEART PHANTOMS

3.1 Introduction

Ventricular septal defects (VSDs) are common congenital cardiac malformations which leave holes between ventricular cavities that alter the blood oxygenation process (Dakkak & Oliver, 2021). For severe VSDs, therapies such as open heart surgery, transcatheter closure, and a hybrid procedure are prescribed. For the latter, occlusive devices are implanted in the septum to close the VSDs. The hybrid procedure comprises a median sternotomy to expose the patient's heart, a puncture in the heart to insert a catheter into it and through the VSD (perventricular intervention), and the device implantation through the catheter. The procedure is performed while the heart is beating and is guided with transesophageal echocardiography (TEE).

To avoid damage of sensitive cardiac tissues during the hybrid procedure, the selection of the puncture site is usually done by palpation. This is because the deformation of the heart due to palpation is clearly observable in TEE. However, maneuvering a catheter inside the heart to access a VSD is not a trivial matter because TEE provides only two-dimensional (2-D) images of a three-dimensional (3-D) anatomical context. Therefore, providing complementary information to the TEE can potentially facilitate the procedure, as has been proven in minimally invasive cardiac interventions for valve repairs (Linte *et al.*, 2009; Moore *et al.*, 2013; Li, Rajchl, Moore & Peters, 2015).

For minimally invasive interventions to repair valves, Linte *et al.* (2009), Moore *et al.* (2013), and Li *et al.* (2015) proposed navigation guidance methods that include 3-D models of cardiac structures and tracking measurements of interventional instruments (including a TEE probe). Relevant information is displayed simultaneously with TEE images in a virtual environment, and in real time. All these methods used an electromagnetic measurement system (EMS), whose miniature sensors were attached to the TEE probe, and other instruments, to collect measurements in and out of the patient's body. While the hybrid procedure presented herein is closely related to the valve repair procedure, with both being performed on a beating heart, the conditions surrounding them are however different. In the hybrid procedure, the patient's heart is exposed for palpation and puncture, which potentially facilitates measurements with sensors outside of the patient's body. If a sensor does not need to be attached to the TEE probe, for example, then that would alleviate concerns related to disinfection and sterilization of the sensor and to physical adaptations of the TEE probe to safely navigate the sensor inside the esophagus of a pediatric patient.

A new navigation guidance method to support cardiologists' actions during a hybrid procedure requires exhaustive evaluations. Such evaluations could include simulations of the procedure in heart phantoms and animal models. Specifically, heart phantoms provide a real alternative for evaluating complex cases prior to a surgical intervention. Indeed, heart phantoms facilitate teaching, training, and planning of treatments (Anwar *et al.*, 2018). Currently, heart phantoms can represent anatomical and physical details with high accuracy thanks to technological advances in both diagnostic imaging (computed tomography [CT], cardiac magnetic resonance [CMR]) and 3-D printing (Yamada *et al.*, 2017). Although the range of materials for printing phantoms directly in 3-D is still limited, classical casting techniques, together with 3-D printing, allow to build heart phantoms made of materials with acoustic properties for ultrasound image acquisition (Morais *et al.*, 2017; Tibamoso-Pedraza *et al.*, 2022).

The contribution of this work is an evaluation of a navigation guidance method to access VSDs in the hybrid procedure. The method includes an EMS, patient-specific heart models, and heart phantoms that represent patient hearts. The EMS allows to track measurements of instruments in the intervention, using sensors that are always outside of the patient's body. The patient-specific heart model is registered with the patient's heart to provide, in a virtual environment, 3-D anatomical information of the VSDs which is not visible to cardiologists using only TEE.

3.2 Materials and methods

In the pre-operative stage of a perventricular intervention, we build a 3-D virtual model of the patient's heart. In the peri-operative stage, we link the virtual heart model with the patient's heart through landmark registration and iterative closest point algorithms. During the intervention, we record the position and orientation of the needle that punctures the patient's heart, and display this information, together with the heart model, in a virtual environment (Fig. 3.1). We evaluate the accuracy of the information provided using a setup we developed to simulate perventricular interventions to close VSDs.

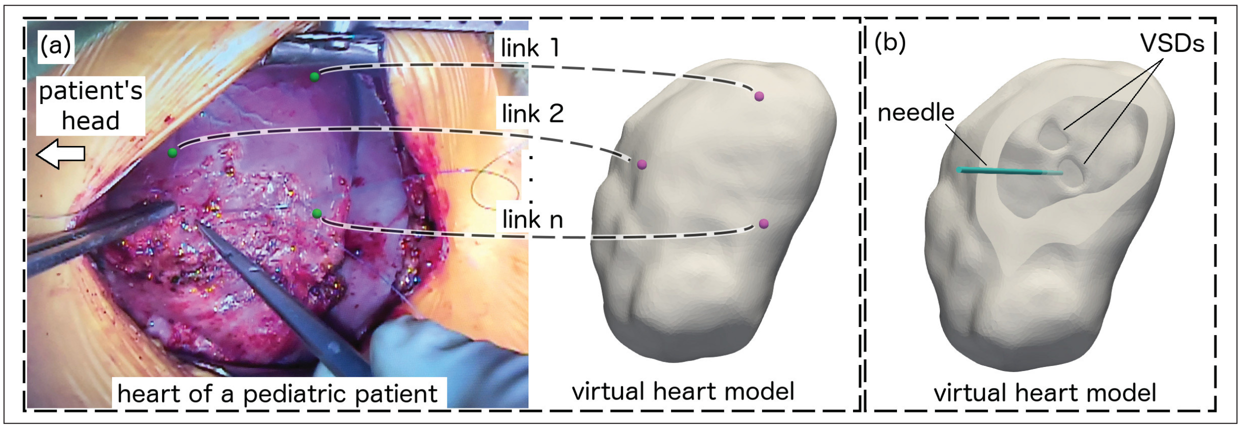

Figure 3.1 Supporting a perventricular intervention to close ventricular septal defects (VSDs) by: (a) linking a patient-specific heart model with the patient's heart, and (b) displaying a needle's puncture with the heart model in a virtual environment

3.2.1 Pre-operative stage: setup for the simulation of perventricular interventions to close VSDs

Our setup simulates the exposure of a patient's heart after a median sternotomy for a perventricular intervention to close VSDs (Fig. 3.2). It includes a patient-specific heart phantom with VSDs, a conduit representing an esophagus, and elements from a real intervention, such as a TEE probe, needles, and guidewires. The setup was designed to reproduce two conditions of a real case: first, the TEE probe is inserted through the esophagus and located beneath the left atrium to acquire images of VSDs in a four-chamber view (Fig. 3.3); second, the right ventricle free wall is exposed for palpation and puncture.

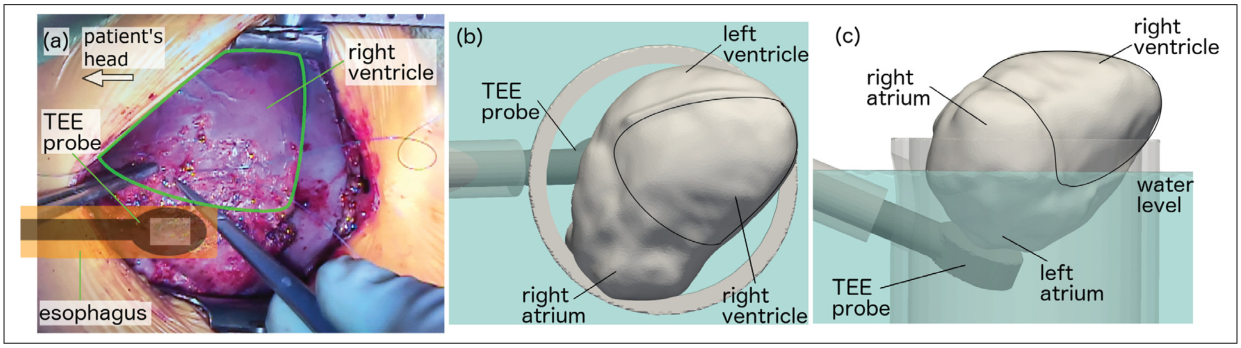

Figure 3.2 Heart exposure for a perventricular intervention to close ventricular septal defects (VSDs): (a) pediatric patient after a median sternotomy; (b) and (c) views of a graphical representation of our setup with a heart phantom

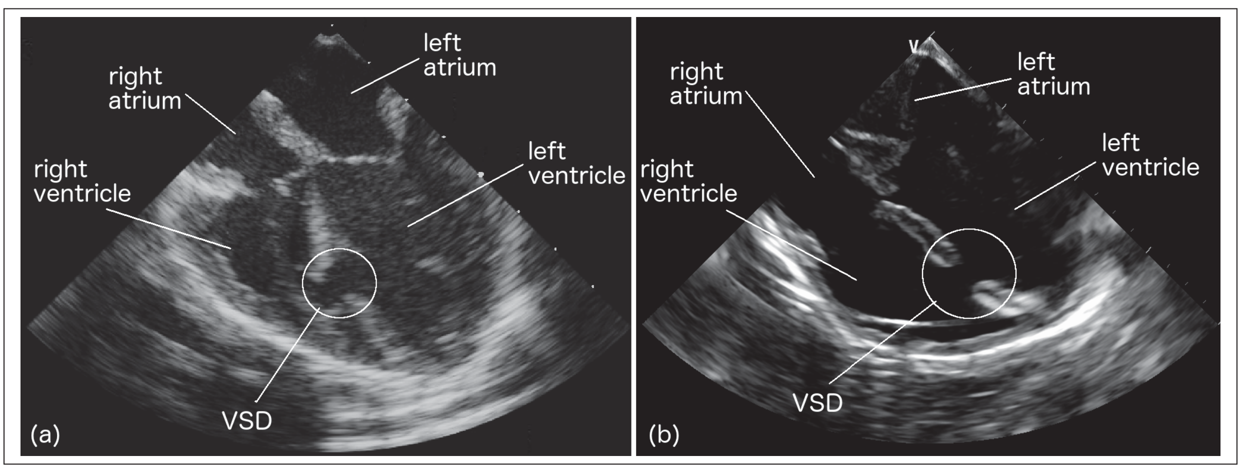

Figure 3.3 Ventricular septal defects (VSDs) in a four-chamber view with transesophageal echocardiography (TEE) from: (a) a pediatric patient, and (b) a patient-specific heart phantom in our setup

In the setup, the heart phantom is placed in a cylindrical support and fastened with two pieces of cotton fabric, with one serving as the phantom's bed, and the other, at the top, which minimizes phantom displacements. Both pieces of fabric have holes that expose the phantom for both image acquisition from the bottom and palpation and puncture at the top. Additionally, spaces between the two pieces of fabric and around the heart phantom were cushioned with small rolls of cotton fabric to restrain displacements of the heart phantom during the simulation.

We connected the heart phantom in a water circuit to maintain an internal pressure to counteract phantom deformations due to palpation or puncture. The pressure was produced by a continuous flow of water inside the phantom. The water flow was maintained by a water pump (MOT-RS-385 12V DC Transparent Water Motor Diaphragm Pump), whose speed was controlled by DC voltage (3 V to 12 V). In the phantom, the water flows from the left to the right cavities (crossing the holes in the septum), which simulates the usual blood flow in a patient's heart with VSDs (Fig. 3.4). We took special care to locate the pump in a dry spot and far from the EMS, avoiding both contact between water and electricity and any disturbance of the EMS measurements. Finally, the phantom's left atrium was submerged in water to create a travel medium for the ultrasound waves coming from the TEE probe. Avoiding air bubbles in the water circuit and inside the heart phantom was important to facilitate ultrasound image acquisition.

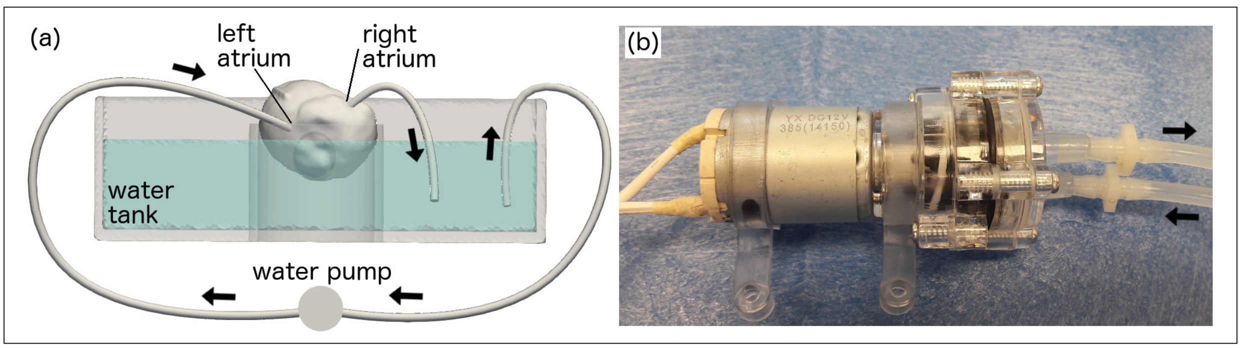

Figure 3.4 A heart phantom in a water circuit: (a) connection of the circuit's components; (b) picture of the water pump used in the circuit. The arrows indicate the water flow direction

3.2.1.1 Patient-specific heart phantoms

We built heart phantoms to represent the cardiac anatomies of two pediatric patients with one and two complex VSDs, respectively. We relied on pre-operative scans (from computed tomography or cardiac magnetic resonance) to reconstruct the hearts' anatomies and to represent them in 3-D virtual heart models. With these models, we designed molds to cast the heart phantoms in PolyVinyl Alcohol Cryogel (PVA-C) following the instructions described in Tibamoso-Pedraza *et al.* (2022), because PVA-C provided good echogenicity for visualization of the phantoms' VSDs in echocardiography.

The heart phantoms represent the size of the patients' hearts in a 1:1 scale, with dimensions of 80 x 65 x 55 mm^3 and 80 x 60 x 50 mm^3 for models A and B, respectively (Fig. 3.5). The VSDs' diameters were estimated to be 7.5 mm for model A, and 6.2 mm and 6.3 mm for model B. The distance between centers of the VSDs in model B was 9.1mm. Reliefs were added on the phantoms' surfaces to mark the boundaries of the ventricular cavities (ventricular septum). In a real case, these boundaries are identified following the path of coronary arteries on the surface of the patient's heart.

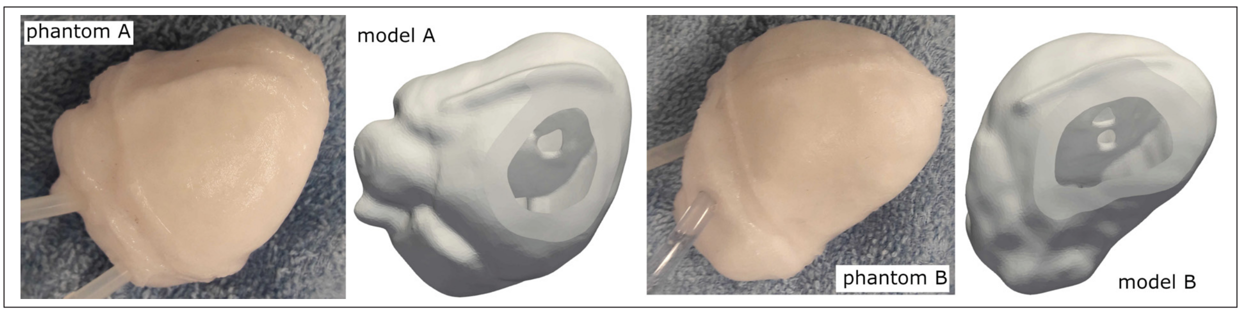

Figure 3.5 Heart phantoms and their respective virtual heart models from two pediatric patients with complex ventricular septal defects (VSDs)

3.2.1.2 Palpation and puncture tools

We used an electromagnetic measurement system (EMS [Aurora V2, NDI, Canada]) with two 6DOF sensors to collect position and orientation information from a palpation and a puncture tools (Fig. 3.6). A EMS sensor was firmly attached to the palpation or the puncture tools using plastic supports that were fixed on the rigid tools.

The palpation tool included a thin plastic conduit with a blunt tip for collecting points on the heart surface. The puncture tool is a collection of a needle and a guidewire; the guidewire goes through the needle to insert a VSD. Initially, for the puncture tool, we used a 21-gauge needle and a guidewire of 0.46 mm diameter; afterwards, we used an 18-gauge needle and a guidewire of 0.89 mm diameter because the bigger diameters of the needle and guidewire facilitates their visualization in ultrasound imaging.

The palpation and the puncture tools were calibrated using pivot and spin calibration implemented in the IGT module of 3D Slicer (Ungi, Lasso & Fichtinger, 2016). In particular, to calibrate the palpation tool we maneuvered a needle such that its tip slightly protruded the conduit's tip (less than 1 mm); we removed the needle after the calibration procedure.

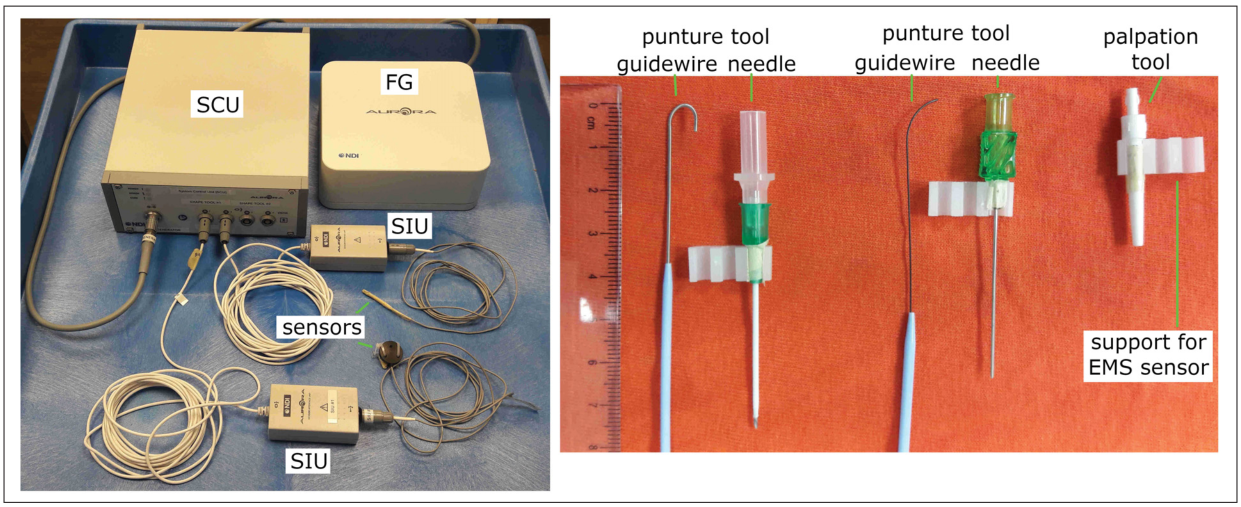

Figure 3.6 Palpation and puncture tools. The electromagnetic measurement system (EMS [Aurora NDI]) includes a field generator (FG), a system control unit (SCU), a sensor interface unit (SIU) and sensors

3.2.1.3 Experimental setup

On a plastic table, we set a water tank (400 mm x 300 mm x 80 mm [length, width, height]) containing a cylindrical support (80 mm diameter, 60 mm height) for a heart phantom. The EMS field generator was also on the table, situated 100 mm from the water tank and 200 mm from the cylindrical support. A 6DOF EMS sensor (reference) was attached to the water tank. A conduit (13 mm internal diameter, 230 mm length), with a tilt angle of -10° with the horizontal, was firmly attached to the water tank to provide a stable support for the TEE image acquisition. Additionally, the conduit's open ends were surrounded with silicone material to increase friction between the conduit and the TEE probe and thereby minimize any unintended motion of the probe. A 4.5 V DC source provided power to the water pump, producing internal pressures of 45 mmHg and 43 mmHg for the heart phantoms with one and two VSDs, respectively. We used a GE Vivid E9 with a 9T pediatric TEE probe for ultrasound (US) image acquisition. The US images were captured and sent to a desktop computer using a DVI2USB 3.0 Epiphan video, while the computer simultaneously received measurements from the EMS. In the computer, the data was recorded at 10 Hz for posterior analysis. We used the PLUS and 3D Slicer software applications for data acquisition, visualization, and interaction (Fig. 3.7).

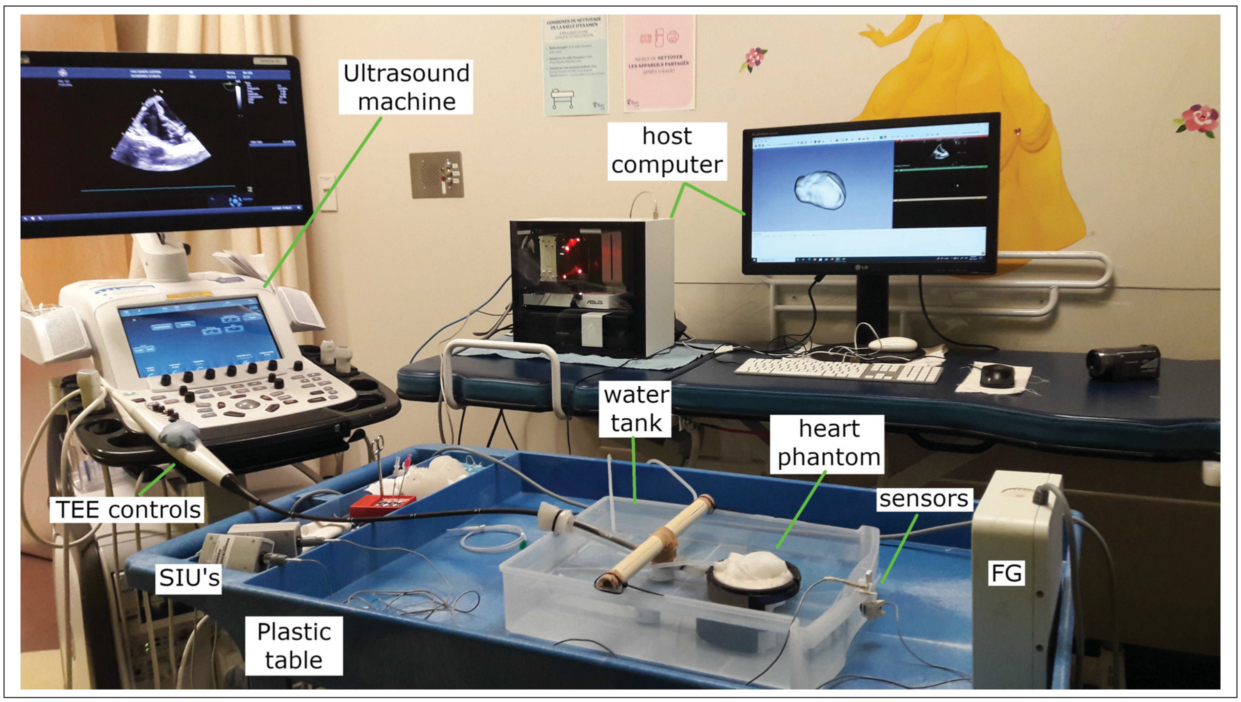

Figure 3.7 Setup for the simulation of a perventricular intervention to close ventricular septal defects (VSDs)

3.2.2 Peri-operative stage: registration algorithms

We have two frames of reference: one for the palpation and puncture tools, and the other for the virtual heart model. To match the two frames, we used a landmark registration algorithm (LR) (Horn, 1987; Ungi *et al.*, 2016). The algorithm requires coordinates of at least three pairs of corresponding points which we manually selected on the patient and virtual hearts (Fig. 3.1 (a)).

For the points' selection, we relied on the atrio-ventricular boundaries (joint region of the heart phantom) and the ventricular septum that protrudes the phantoms' surface.

The result of the LR consisted of a set of geometric transformations (translations, rotations, and uniform scaling) that map coordinates from one frame of reference to the other. Therefore, the position and orientation of the palpation and the puncture tools with respect to the patient's heart were mapped–using the resultant transformations–to accurately represent the same geometrical relations between the tools and the heart model in the virtual environment. We included scaling in the geometric transformations to consider that the heart's size of a pediatric patient could change from the moment of the pre-operative scanning until the moment of the hybrid intervention (several weeks of difference).

We also tested an iterative closest point algorithm (ICP) to fine-tune the mapping results achieved with the landmark registration counterpart. It is generally suggested to feed the ICP with coordinates from 30 to 40 pairs of corresponding points. For the ICP, we manually selected points evenly distributed on the right ventricle free wall of the patient's heart. Afterwards, the corresponding points on the virtual heart model were automatically selected by calculating the minimum distance between each manually selected point and the virtual heart model. The ICP produced a set of geometric transformations that included translations and rotations.

The procedures described in this section were applied with the Fiducial Registration Wizard and Fiducials-Model Registration modules of SlicerIGT in 3D Slicer (Ungi *et al.*, 2016). We used the palpation tool to select the points on the surface of the patient's heart and a computer mouse for those on the virtual heart model.

3.2.3 Intra-operative stage: perventricular intervention to access a VSD

Two cardiologists performed perventricular interventions on the heart phantoms (patient's heart) following exclusively the information displayed in the virtual environment for guidance. In the virtual environment, the position and orientation of the VSDs in the patient-specific virtual heart model were clearly visible, as was a representation of the puncture tool, which followed the actions of the physical one in real time.

Following the information displayed in the virtual environment, a cardiologist maneuvered the puncture tool to puncture the heart (right ventricle free wall) and access a target VSD of a heart phantom in two ways: first, crossing the VSD directly with the needle, and second, crossing the VSD with the guidewire that goes through the needle. The second way more closely approximates what is practiced in a real intervention, where a needle punctures and accesses the heart, but the needle's tip is positioned in between the puncture site and the target VSD. Results of the VSD accesses with the needles and guidewires were evaluated scanning the heart phantoms with TEE.

3.2.4 Experiments

We conducted a series of experiments to evaluate the information provided in the virtual environment for guidance to access VSDs. Three registration cases were evaluated. In the first case, we applied the landmark registration algorithm (LR) with seven fiducials (landmarks). In the second, we applied LR with three fiducials and the iterative closest point algorithm (ICP) with seventy points. Finally, we applied LR with seven fiducials and ICP with forty points.

3.3 Results

3.3.1 Registration results

Fig. 3.8 shows the results of the registration methods, with dots in red representing fiducials selected on the virtual heart models; dots in green representing mapping results with the LR applied to fiducials selected on the heart phantoms, and dots in blue represent mapping results with the ICP applied to the dots in green (cases two and three). Registration error measurements were calculated using the Euclidean distance between corresponding fiducials, i.e. between red and green dots in the case one, and between red and blue dots in the cases two and three (Table

3.1). A detailed description of the results, which are discriminated by the three registration cases, is presented as follows.

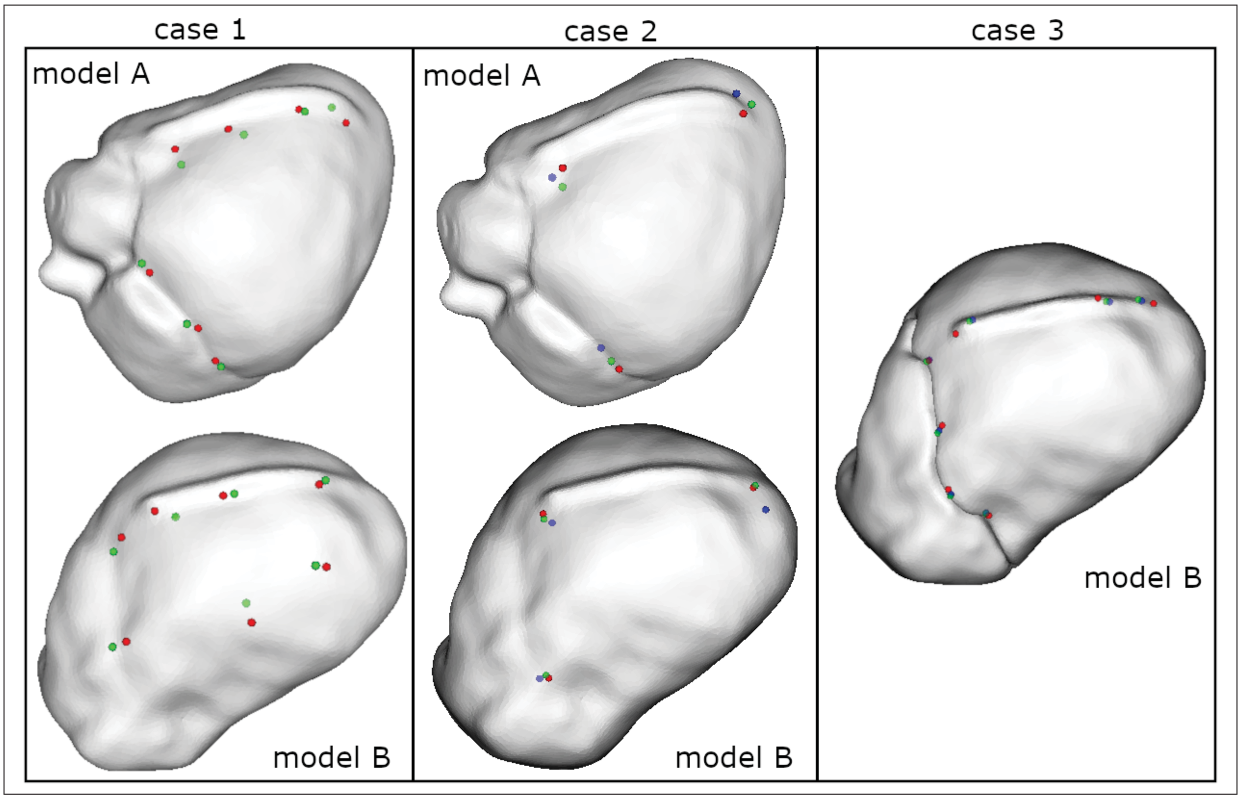

Figure 3.8 Registration results of fiducials selected on the virtual heart models (red) and after applying the landmark registration (green) and iterative closest point (blue) algorithms to fiducials on the heart phantoms

Table 3.1 Error measurements using the Euclidean distance between corresponding fiducials after registration using a landmark registration algorithm (LR) and an iterative closest point algorithm (ICP)

case	heart model	number of fiducials	registration algorithms	error (mm)				
				min.	max.	rms	mean	std.
1	A	7	LR	1.17	3.46	2.30	2.19	0.70
1	B	7	LR	1.26	3.77	2.69	2.56	0.84
2	A	3	LR and ICP	2.34	4.82	3.93	3.79	1.06
2	B	3	LR and ICP	2.63	4.89	3.70	3.57	0.96
3	B	7	LR and ICP	0.68	4.08	2.28	2.00	1.10

3.3.1.1 Case 1: LR with seven fiducials

For heart model A, we observed a better registration accuracy for landmarks located on the atrioventricular border than along the septum (Fig. 3.8, case 1, model A). For the heart model B, we noted an evenly distributed error between most of the fiducials (Fig. 3.8, case 1, model B); fiducial selection on the atrioventricular border was limited because of an unclear border definition, which affected the overall accuracy (2.69 RMS error, Table 3.1). For both heart models (A and B), we noted that the uniform texture and color of the phantoms and the virtual models hindered an accurate selection of fiducials.

3.3.1.2 Case 2: LR with three fiducials + ICP

For both hearts, we noted that the registration errors increased after the ICP was used, i.e., the distances between red and blue dots were larger than those between red and green ones (Fig. 3.8, central column). A low consistency in the results before and after using the ICP indicates that three corresponding fiducials are not enough: a limited number of fiducials on deformable bodies (heart phantoms) makes the registration highly sensitive and prone to errors (3.93 and 3.70 RMS errors, Table 3.1).

3.3.1.3 Case 3: LR with seven fiducials + ICP

For heart B (two VSDs), we tested LR and ICP, selecting seven corresponding fiducials. To facilitate landmark selection, the atrioventricular border and the septum on the heart phantom were painted (using a waterproof marker pen), and the virtual heart model was represented by two sections, atriums and ventricles, highlighting boundaries (Fig. 3.9). Landmarks registration consistency with and without the ICP suggests that the landmark selection was accurate (Fig. 3.8, right column). The RMS error of this case was the lowest (2.28 RMS error, Table 3.1).

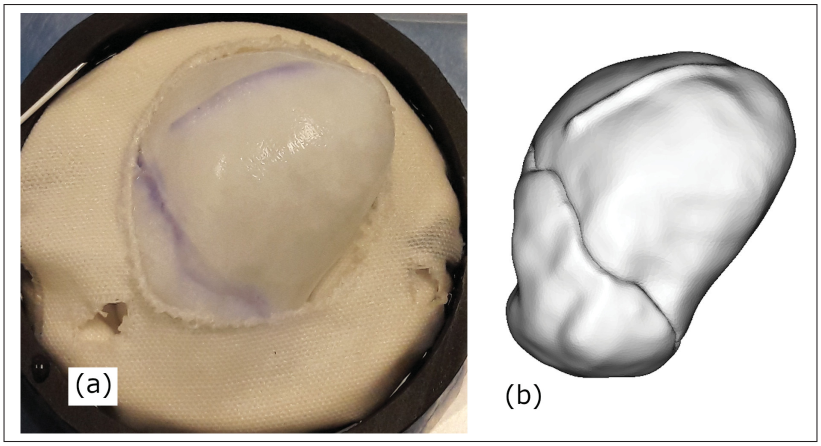

Figure 3.9 Anatomical details enhancement for the selection of corresponding fiducials on: (a) a heart phantom, and (b) a virtual heart model

3.3.2 Accessing VSDs with the puncture tool guided by the virtual environment

In each case, after the registration of the virtual heart model with the heart phantom, punctures on the heart phantom were performed to access a target VSD. For each puncture, a cardiologist selected both a puncture site on the right ventricle free wall and the orientation of the puncture tool, following exclusively the information displayed in the virtual environment. The success or failure to access the target VSD with the puncture tool was evaluated monitoring the VSD with TEE (Fig. 3.10).

The cardiologists inserted the target VSDs with the puncture tool, using a needle and a guidewire (Fig. 3.11). We noted that the needles were inserted in the target VSDs more easily than did the guidewires–a guidewire has a curved head. Nevertheless, accessing the VSDs with the guidewires is more significant than with the needles, because the former closely represent what is practice in a real intervention. Table 3.2 summarizes the results of inserting the puncture tool on the target VSDs (one VSD in heart A and two VSDs in heart B).

We noted that accessing target VSDs in the model B was more difficult than in the model A; the closeness of the VSDs in the model B increased the difficulty to accurately insert a target VSD and avoid to insert the other one. Therefore, the results accessing the VSDs in the model B

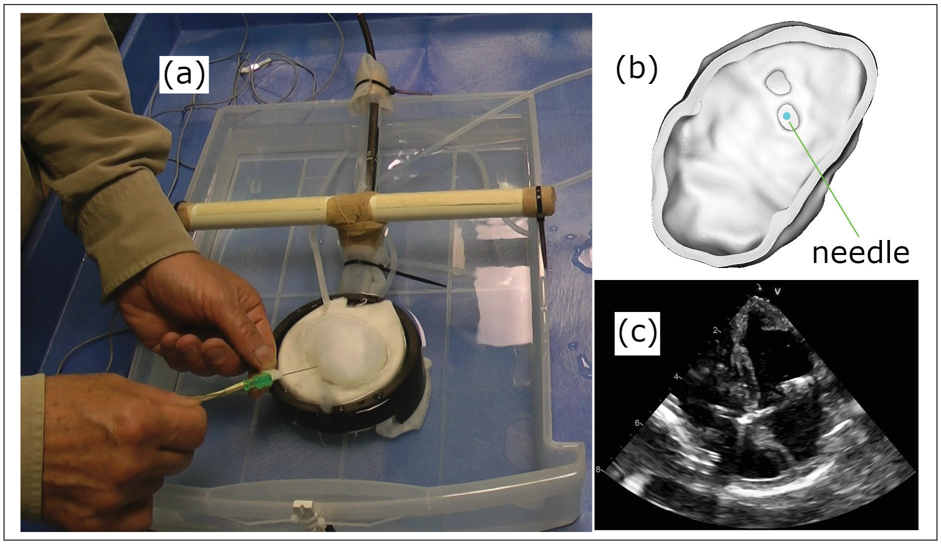

Figure 3.10 A cardiologist performing a perventricular intervention to access a VSD in a heart phantom: (a) experimental setup, (b) virtual environment for guidance, (c) TEE images for evaluation

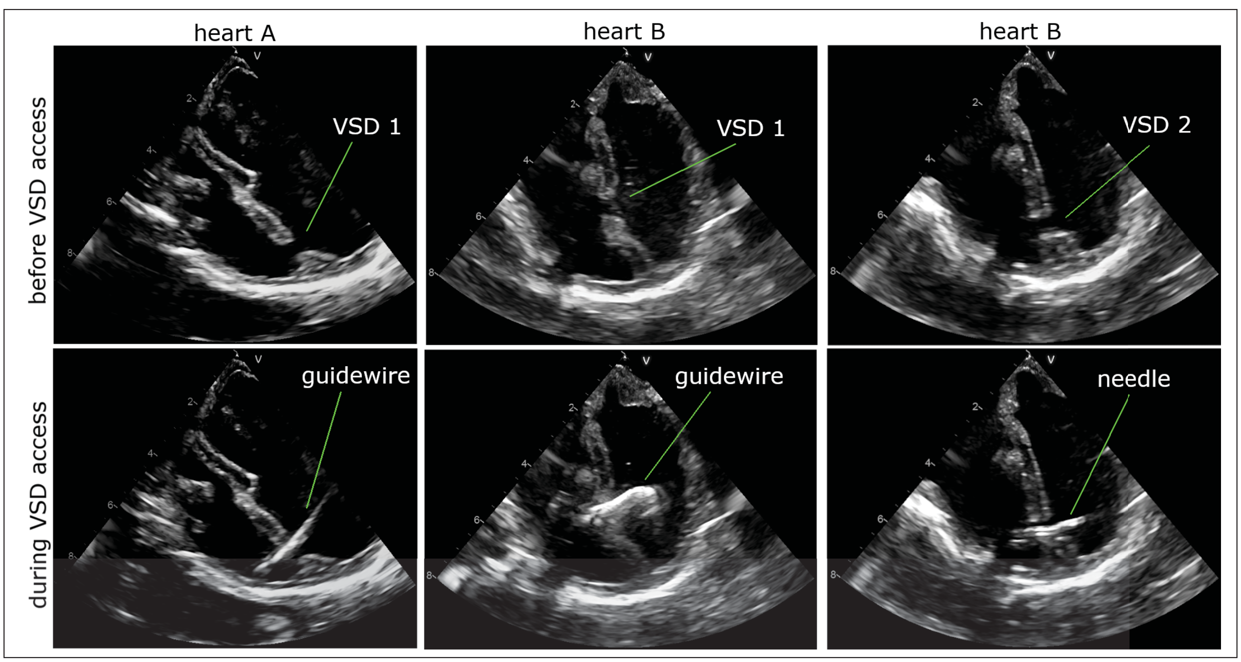

Figure 3.11 Frames of TEE from the two heart phantoms before and during VSD access with a needle (heart B-VSD2) and a guidewire (heart A and heart B-VSD1)

Table 3.2 Perventricular intervention results from accessing VSDs in the heart phantoms with needles and guidewires. For each fraction, the denominator indicates the total number of attempts, and the numerator, the number of successful accesses to the respective VSDs

case	heart model	VSD	needle	guidewire
1	A	1	1/1	1/2
1	B	1	2/2	1/3
1	B	2	6/8	1/3
2	A	1	3/4	1/3
2	B	1	0/0	0/2
2	B	2	0/0	0/1
3	B	1	1/1	3/3
3	B	2	4/4	4/4

are more significant than those in the model A. From those results, we noted that a registration error of 3.70 mm RMS (case 2, heart model B) was too high because none of the three attempts with guidewires (two for VSD 1, and one for VSD 2) reached the targets (Table 3.2). In contrast, the enhancement of anatomical details (case 3) improved the registration results (2.28 mm RMS error), as well as the perventricular access accuracy, where all seven attempts with the guidewires reached the targets (three for VSD 1, and four for VSD 2).

3.4 Discussion

With the simulation setup we developed, we found that a patient-specific virtual heart model together with an electromagnetic measurement system (EMS) provide relevant and complementary information to support guidance during a perventricular intervention to close ventricular septal defects (VSDs). A high confidence for intervention guidance was achieved when seven corresponding fiducials were selected on clearly identified anatomical landmarks for the registration of the heart phantom (patient's heart) with the virtual heart model.

Despite the limited number of cases, we noted that a registration error of 2.28 mm RMS was acceptable to insert VSDs of at least 6.2 mm diameter (case 3). Those results were achieved thanks to a clear demarcation of anatomical details along the atrioventricular border and the septum that facilitated the selection of landmarks for the registration of the heart phantom with the virtual heart model.

In a real intervention, anatomical details, along the atrioventricular border and the septum, could be identified following the path of coronary arteries that are exposed after a median sternotomy. Therefore, we recommend highlighting coronary arteries during the pre-operative scan acquisition, which could facilitate image segmentation and 3-D reconstruction of these anatomical structures in a patient-specific virtual heart model. Additional anatomical landmarks could be considered such as roots of the pulmonary artery and aorta.

The iterative closest point algorithm (ICP) aims to fine-tune the results obtained with the landmark registration algorithm (LR). For case 3, for example, ICP fine-tuned the needle position by 0.5 mm (where 0.3 mm was a correction of the needle's depth), and its orientation by 1.23 degrees. Nevertheless, we consider those fine-tuned values small and, in a real case of a perventricular intervention, collecting 30 to 40 points from a deformable and moving heart for the ICP could be a complex task and one that is prone to errors. Therefore, we suggest to avoid ICP and to rely on an accurate landmark selection for the LR.

We introduced uniform scaling in the transformation matrix to consider possible changes of the heart's size over time. However, this assumption could be problematic considering that the heart's size could change in a non-uniformly way, e.g. the left ventricle grows faster that the rest of the organ, which could affect the registration accuracy. It remains to be seen how the size of a heart with VSDs changes over time, to evaluate alternatives for scaling.

We limited our study to analyzing spatial information when the heart is static. Nevertheless, simulating the heart in motion–including the atrioventricular valves–is the next step to observe more similarities with a real case. This would also imply synchronizing the spatial measurement information provided by the EMS with the cardiac cycle and selecting those values at the end of diastole, when the VSD sizes are largest. Future work will include cardiac cycle identification from images captured from outside (using a video camera) or from inside (TEE) hearts with VSDs.

The experience of cardiologists in our team was essential in the design of the experimental setup, considering the requirements and conditions of a real intervention. Accordingly, we are confident that the results from our experiments represent a successful proof of concept for navigation guidance in the hybrid procedure; however, a generalization of the proposed method requires a more extensive cohort of pediatric patients with VSDs, allowing to consider multiple heart shapes, sizes, and malformations due to defects. The developed setup is flexible and permits the addition of more cases, and further, could be adapted for training and planning purposes.

In the proposed setup, the cardiologists received simultaneous information from a host computer, the TEE machine, and the patient's heart during the hybrid intervention. We believe that additional devices, such as Microsoft HoloLens, could make it easier to visualize and interact with information from several sources at the same time. Future work could evaluate the feasibility of these devices in the hybrid procedure.

CHAPTER 4

CARDIAC MOTION TRACKING IN ULTRASOUND IMAGING OF VENTRICULAR SEPTAL DEFECTS

4.1 Introduction

Ventricular septal defects (VSDs) are common congenital cardiac malformations (Penny & Vick, 2011). VSDs are mostly due to incomplete development of the ventricular septum, leaving holes between ventricular cavities that disturb the normal cardiac function. Small holes do not present major problems and regularly close in the course of time, but large ones require surgical treatment. Open heart surgeries or catheter-based interventions are usually performed to close VSDs.

Characterizing VSDs is an important step for diagnosis and treatment; characteristics of a VSD include size, position, orientation, shape, and surrounding tissues. Medical image modalities such as X-ray, computed tomography (CT), cardiac magnetic resonance (CMR), and echocardiography play a fundamental role no only for VSDs characterization but also for intervention planning. In particular, transesophageal echocardiography (TEE) is highly relevant for a VSD characterization, intervention planning, and intervention guidance, because TEE provides images of the beating heart in real-time through a TEE probe that is inserted in the patient's esophagus.

For VSDs characterization, cardiologists choose the end of diastole to measure sizes of VSDs. In a cardiac cycle, the end of diastole occurs when the ventricular cavities are completely expanded; additionally, it is at the end of diastole that the VSDs show their biggest sizes. Our goal is to evaluate a new semi-automatic method to track boundaries of the ventricular cavities of hearts with VSDs in ultrasound imaging (TEE); tracking cardiac boundaries will help to identify the end of diastole of each cardiac cycle. The method relies on particle filtering, which is known to be robust in the presence of noise, artifacts, and diffuse and incomplete boundaries of tissues in ultrasound images (Laporte & Ménard, 2018; Carneiro & Nascimento, 2013). Our method controls size, position, and orientation of two ellipses to follow right and left ventricular boundaries even in cases where the ventricles are partially visualized.

4.1.1 Related work

Motion tracking of soft tissues in ultrasound images has been a challenging and still an open problem (Ouzir, 2018). The challenges include noise, artifacts, and diffuse boundaries of biological tissues. Additionally, the organs move in a three-dimensional (3-D) space, but the acquired images are in two dimensions; the limited field of view of ultrasound imaging makes the motion tracking an ill-posed problem. Introducing regularization constraints is a common practice to reduce complexity for the cardiac motion estimation, and to achieve outcomes with spatial and temporal smoothness (Ouzir, 2018).

Block matching, optical flow, and elastic registration are common methods of cardiac motion estimation (Ouzir, 2018). These methods look for similarities between two consecutive frames to determine a dense motion field. Estimating a dense motion field, however, could be computationally expensive. Alternative methods include tracking selected features such as image boundaries (Dietenbeck *et al.*, 2014; Carneiro & Nascimento, 2013; Laporte & Ménard, 2018). Within these alternatives, particle filtering has been one of the appealing approaches (Carneiro & Nascimento, 2013; Laporte & Ménard, 2018), given its flexibility to use prior information, its capacity of adaptation to the image features (like possible alterations of movement due to biological factors and pathological conditions), and its simple and elegant formulation that allow an efficient computational performance.

4.2 Methods: Motion tracking in TEE

Our method consists of automatically attach curves to the ventricular walls and septum during beating heart in ultrasound imaging of mid esophageal four-chamber view. Each curve is manually initialized in a selected frame and automatically updated for the following images of the sequence by particle filtering. The filter predicts the curve parameters (posterior), based on probable cardiac motion (prior), and both intensity image distributions and geometrical constraints (likelihood), supported by training data. A more detailed description of the system components is presented as follows.

4.2.1 Training data

We rely on training data to extract motion information. On TEE image sequences, we interactively approximate the shape of the left and the right ventricle walls with two curves of elliptical shape, as shown in Fig.4.1. The parameters that define each curve, namely its center (c_x, c_y), length of long and short axes (a, b), and tilt angle (θ), define a feature vector. Each feature vector is expressed with respect to a coordinate reference system defined by two anatomical landmarks (apex and base), which are the extreme points of the ventricular septum as shown in Fig. 4.2. These landmarks are manually defined in one selected frame, and the distance between these two points is used to normalize the values of the center and axes length. We propose to choose the selected frame at the end of diastole, when the heart expansion is maximum, in order to have a common reference between different sequences. Afterward, we calculate the arithmetic difference between feature vectors of each two consecutive frames, obtaining feature vectors of $[\Delta c_x, \Delta c_y, \Delta a, \Delta b, \Delta\theta]$, and from these we model each Δ component as a zero-mean Gaussian distribution, for both the left and right ventricles.

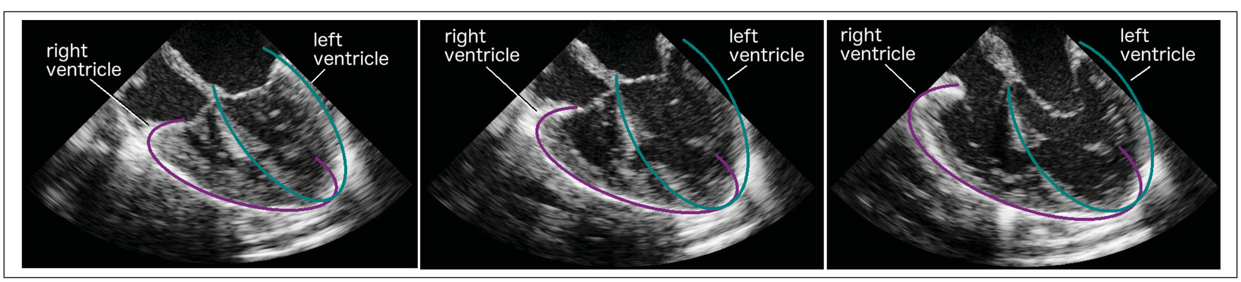

Figure 4.1 Approximation of left and right ventricle walls with two elliptical shape curves in TEE images of four chamber view. Note that the curve for the left ventricle includes the septum and that in some cases parts of the curves are outside of the field of view

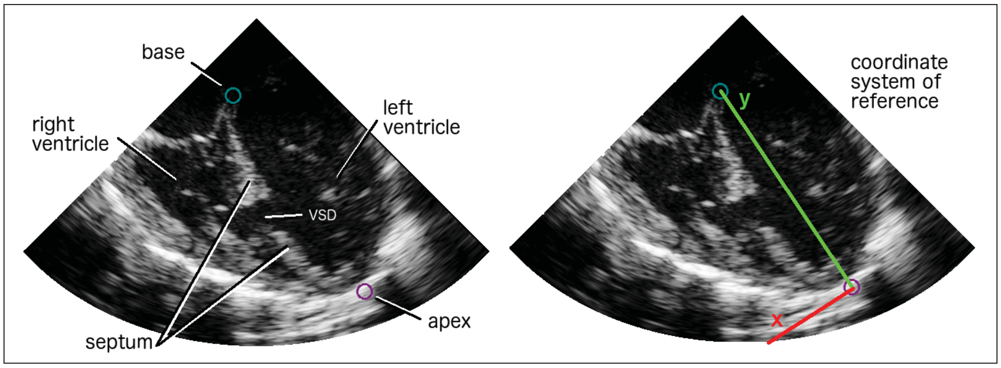

Figure 4.2 The coordinate reference system for the elliptical curves defined using the apex and base landmarks

4.2.2 Particle filtering

For each frame, a particle filter generates random samples of curves from prior information that could describe the boundaries of the right and left ventricles, and evaluates these samples with information from the image, in order to predict the curves that best describe the borders of interest. The sample generation depends on parameters set in the first frame of the sequence, prior motion behavior collected from the training data, and predictions of the previous frame. Fig. 4.3 shows the steps of this process. Related functions are described as follows.

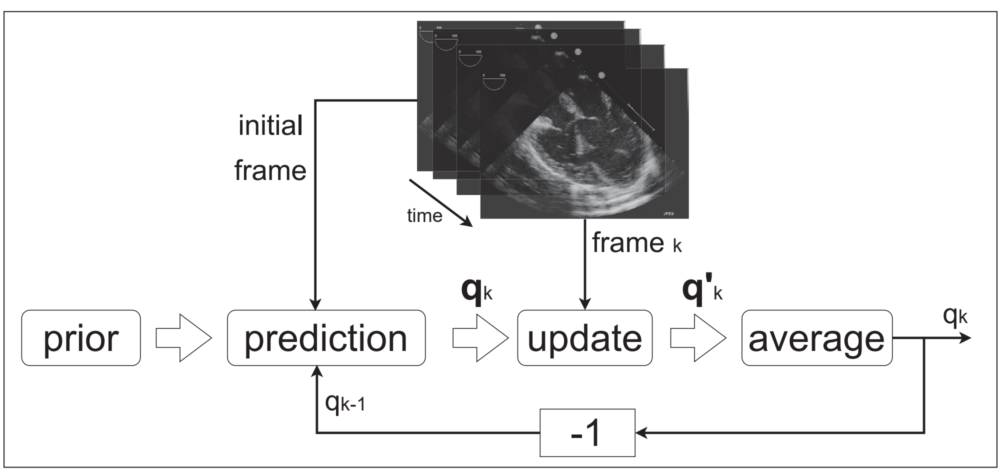

Figure 4.3 Diagram of the particle filter method for cardiac motion tracking in transesophageal echocardiography (TEE).

4.2.2.1 Initialization

Two main parts compound the initialization step. The first one consists of outlining the right and left ventricles interactively with two curves of elliptical shape, on a selected frame at the end of diastole ($initial\_frame$), as is shown in Fig.4.4. In the same frame, the apex and base points are selected, with which a coordinate system of reference is defined. Hence, each curve is represented by a feature vector ($initial\_feature\_vector$), composed of five parameters [c_x, c_y, a, b, θ], where the first four of them are normalized with respect to the apex-base distance. These feature vectors are copied to initialize two sets of particles, for the left and right ventricles. The number of particles (N) is defined experimentally.

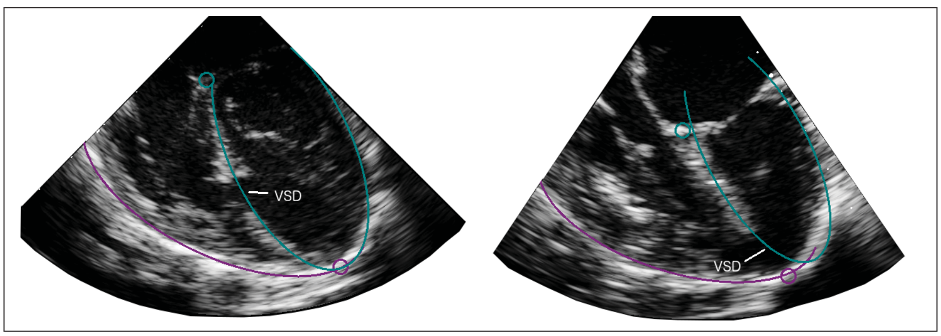

Figure 4.4 Elliptical curves initialization in TEE images at the end of diastole from patients with VSD

The second part consists of defining two constraint values from the selected frame, restraining the expansion of the curves further than their initial definition at the end of diastole (selected frame). The first constraint is the area enclosed by each one of the initial curves (elliptical shape), calculated as $initial\_area = \pi * a * b$. The second constraint is the number of pixels with intensity values above a threshold that are enclosed by each one of the initial curves ($initial\_pixels\_area$). The threshold is defined interactively, where the user chooses regions at the border of the right ventricle and the septum, as is shown in Fig. 4.5. With this information, we extract median values of the region intensities that we call $median\_rv$ and $median\_septum$, which are the thresholds for the right and left ventricles, respectively. These parameters are used in the update step.

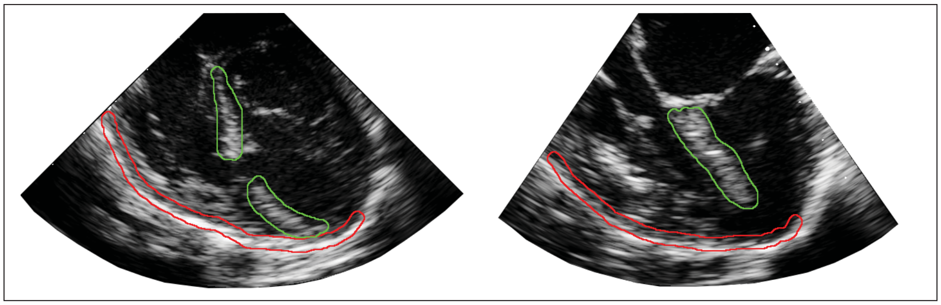

Figure 4.5 Region selection from the ventricle border (red) and the septum (green) in order to define the thresholds

4.2.2.2 Prediction

For each frame, the prediction step drives the particles toward probable borders of the right and left ventricles, based on prior motion extracted from the training data (zero-mean Gaussian distributions of Δ components) and the initial parameters for each curve defined in the first frame. We define the prediction step as

$$q(i)_k = q(i)_{k-1} + r_i - h(i), \tag{4.1}$$

where q is a particle, i is each component of the particle, k the frame number, r_i is a random value drew from the zero-mean Gaussian distribution for the component i, and $h(i)$ is a function defined as

$$h(i) = (q(i)_{k-1} - initial\_feature\_vector(i))/m, \tag{4.2}$$

where m is the number of frames per cardiac cycle. The reason why we include initial_feature_-vector(i) in eq.4.2 as a constraint is because of the assumption that the ventricular walls revisit initial positions during each cardiac cycle. On the other hand, for our experimentation the value of m is defined according to the number of TEE frames per beat for each case.

4.2.2.3 Update

In this step, the components of each particle (q) are used to reconstruct the respective curve (elliptical shape) over the image, and evaluate it in order to give to this particle a score by

$$score(q) = tissue(q) * ratio\_area(q) * ratio\_pixels\_area(q), \tag{4.3}$$

where $tissue(q)$ calculates the percentage of the curve that is inside of cardiac tissues (right ventricle wall, or septum and left ventricle wall), namely the percentage of points along the curve that correspond with pixel values above the threshold defined in the initialization step. The $ratio\_area(q)$

$$ratio\_area(q) = min(\frac{area(q)}{initial\_area}, \frac{initial\_area}{area(q)}), \tag{4.4}$$

and $ratio\_pixels\_area(q)$

$$ratio\_pixels\_area(q) = min(\frac{pixels\_area(q)}{initial\_pixels\_area}, \frac{initial\_pixels\_area}{pixels\_area(q)}) \tag{4.5}$$

constrain the curves to a maximum area but preserving similar intensity distribution inside it. The values of $score$ are between $[0, 1]$, which are weighted through a Gaussian curve with mean 1 and standard deviation of 0.2, and normalized with respect to the sum of the $scores$ of all the particles, and therefore converting them into probabilities.

To work properly, a particle filter requires resampling (Gustafsson, 2015). Resampling is applied when the weights of a considerable number of particles are practically zero. We evaluated this condition in every epoch, using the effective number of particles (N_{eff}),

$$N_{eff} = \frac{1}{\sum_{i=1}^{N}(scores(i))^2}. \tag{4.6}$$

The N_{eff} indicates how many particles are contributing with the prediction. For example, when only one particle contributes with the prediction, i.e. $scores = 1$ for one particle and $scores = 0$

for the rest, $N_{eff} = 1$; conversely, when all the particles contribute with the prediction, i.e. $scores = 1/N$ for every particle, $N_{eff} = N$. We applied resampling when $N_{eff} < N/2$.

After the update step, the actual output is the arithmetic average of the particles for each ventricular cavity.

4.3 Experimental methodology

4.3.1 Training data

We manually fitted ellipses to the ventricular borders in TEE image frames of four chamber view, extracting the information required to build the prior from 52 consecutive frames of a pediatric patient with VSDs, which in total comprised five heartbeats. The 2D images were acquired with a Phillips IE33 Ultrasound Machine with a frame rate of 78 Hz, depth of 8.1 cm, the pixel size of 0.17 x 0.17 mm^2, and image size of 800 x 600 pixels.

4.3.2 Validation data

We validate our method on two clips of TEE image acquisitions of four chamber view from two pediatric patients with VSDs. The clips comprised four and three heartbeats, which were acquired with frame rates of 87 Hz and 102 Hz, respectively. Both TEE image sequences were acquired using a Phillips IE33 Ultrasound Machine with pixel size of 0.15 x 0.15 mm^2 and image size of 800 x 600 pixels.

We compared the tracking results with manually delineations of the heart boundaries, i.e. the external right and left ventricle walls (epicardium) and the center line of the septum were delineated through all frames of the two validation sequences. The delineation was made for the first author of this paper, taking into account advice from experts in this imaging modality. In Fig.4.9 are shown some of the manual delineation results.

4.3.3 Particle filter parameters

We evaluate the performance of the filter with 10, 20, 50, 100, and 150 particles, with the same initialization parameters extracted from a selected image frame–end of diastole–in each case. We defined m according to the number of frames per heartbeat in every clip. For the first and second cases, we set m=10 and m=40, respectively, which approximately correspond with the number of frames per cardiac cycle in each case.

4.3.4 Accuracy measures

To evaluate tracking accuracy, we estimated the average distance between the prediction and the reference curves. In order to obtain this measure, we trace straight lines from the center of the prediction curve (ellipse) in all directions. Every time that a line touch the reference and prediction curves, we calculate the Euclidean distance between the touched points ($d1, \ldots, dn$), as it is represented in Fig.4.6. The average of the distances is obtained for each of the reference segments, namely right and left ventricles, and septum. For this case, we define 2 degrees the value of the angle between two consecutive lines.

4.4 Results and Discussion

Tracking results are presented in Fig. 4.7, which suggests that the filter get stabilization after 50 particles. Additionally, quantitative results of an average distance less than 2 mm in all the experiments show a good performance in the tracking of our method. Execution time is approximately 1 s/frame when we use 150 particles in a desktop computer with a 3.1 GHz Intel Core i7 processor and 16 GB in RAM.

Qualitative results indicate that the filter can overcome problems when there is missing image information (Fig.4.8). This property is due to the constraints included in the prediction and update steps of the particle filter, namely initial areas and position of the curves. Nevertheless, in some cases these constrains become the method too restrictive, missing adaptability to the

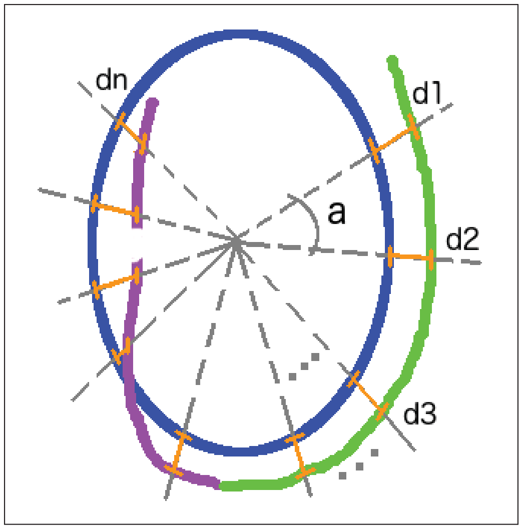

Figure 4.6 Graphical representation of distance estimations between the prediction (blue) and the reference curves (green and purple). The a is the angle between two adjacent line segments.

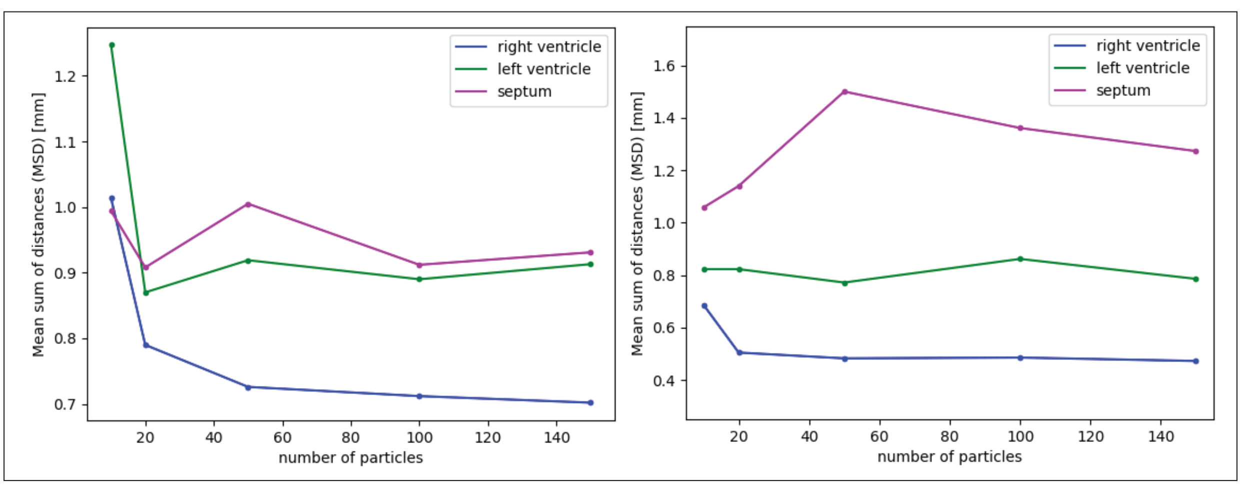

Figure 4.7 Average distances between the prediction and reference curves for the right and left ventricle walls, and septum for each of the two TEE validation sequences. We ran experiments with 10, 20, 50, 100, and 150 particles

septum shapes (Fig.4.9). We think we could reduce constraints if we first track the right and left ventricle walls, and then we track the septum inside the area limited by the former result.

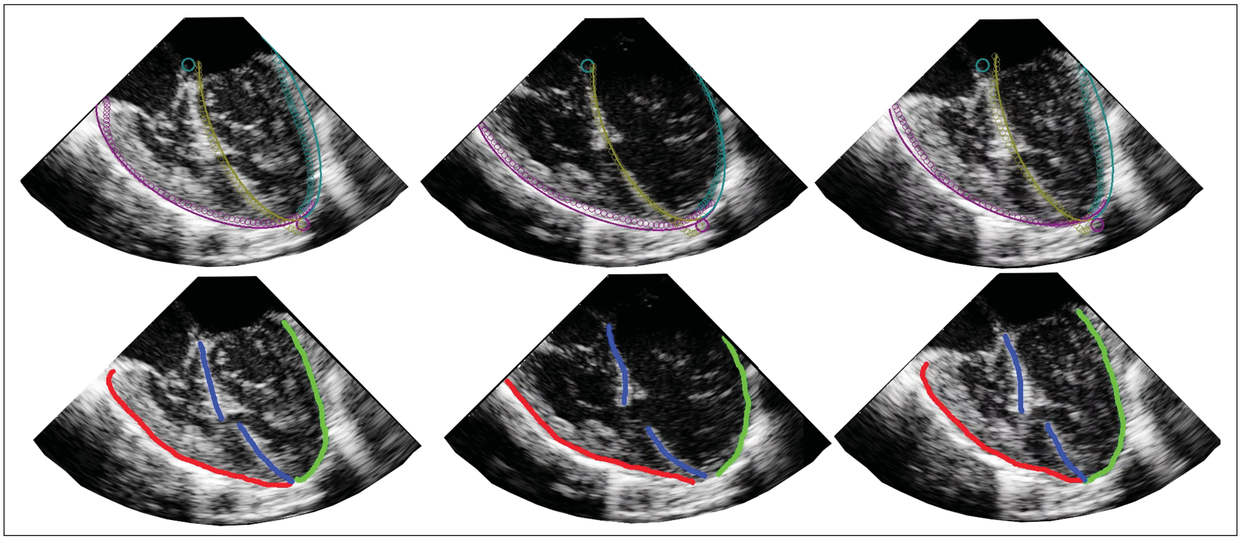

Figure 4.8 Qualitative results from the first validation sequence. (Upper row) Curves in magenta, blue, and yellow are results of the tracking in images of a TEE sequence. (Bottom row) Same images from the upper row with manual tracing as the reference of the external right (red) and left (green) ventricle walls (epicardium), and the septum center line (blue)

Representation of the ventricular walls by ellipses is initially attractive because of the regular shape of these structures in newborns, and also because the curves are represented with a minimum number of parameters. However, we think a more flexible curve representation is required in order to include shape variations as in the case of VSD. B-splines or Active Shape Models (ASM) are potential alternatives.

We chose a threshold of intensity values from the TEE images in order to evaluate the likelihood of each particle. One of the reasons for this is that the threshold allows extracting regions close to the boundaries of the cardiac structures. In addition, the threshold is estimated from a manual segmentation, and therefore adaptable to the specific TEE sequence. However, the intensity values in the ultrasound images depend on the tissue orientation with respect to the TEE probe. Additionally, the segmentation depends on the familiarity of the user with the TEE images. We think the method could be more accurate if we consider the TEE intensity patterns

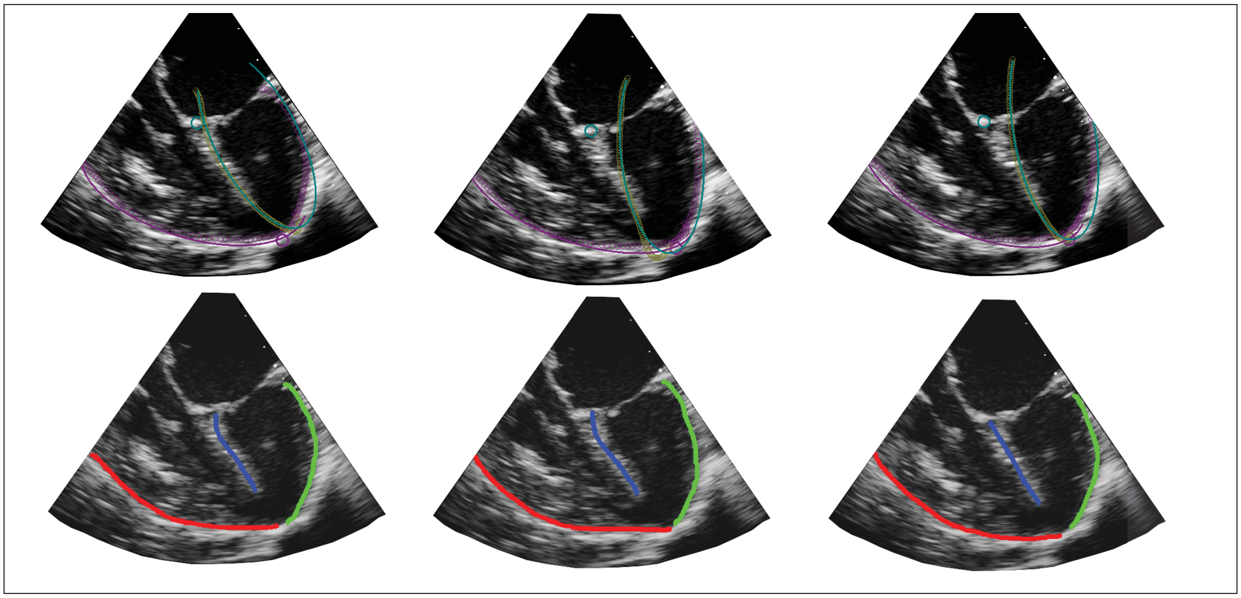

Figure 4.9 Qualitative results from the second validation sequence. (Upper row) Curves in magenta, blue, and yellow are results of the tracking in images of a TEE sequence. (Bottom row) Same images from the upper row with manual tracing as the reference of the external right (red) and left (green) ventricle walls (epicardium), and the septum center line (blue)

of the ventricles into the method, maybe through active appearance models (AAM) or machine learning techniques.

We acknowledge limitations of our results due to the limited number of cases for training and validation purposes. An increasing number of cases could provide a better picture of the potential of particle filtering for motion tracking of the heart with VSDs in ultrasound images. To overcome this limitation, collecting data from different institutions and from different patients would be advantageous to strength the statistical and probabilistic analysis that support the results of the proposed methods.

The proposed accuracy measure could lack uniform distribution of intersections along the predicted and reference curves. As an alternative, the method results could be evaluated comparing two ellipses, one that represents the prediction and the other that is manually fitted on the ventricular borders, for each frame. In this way, the evaluation would be simplified comparing the parameters (features) that define every ellipse.

4.5 Conclusion

We have proposed a semi-automatic method to track the ventricular part of the heart with VSD from TEE sequences. The method has shown good accuracy tracking the ventricle free walls, but the accuracy is reduced in the case of the septum. Future works will include curve representation with more flexibility, constrains reduction, and explorations of feature extraction from TEE with techniques from machine learning. This tracking could support diagnostic analysis and navigation guidance for VSD-closure.

CONCLUSION AND RECOMMENDATIONS

Ventricular septal defects (VSDs) are common congenital heart malformations. Large VSDs require surgical treatment. In newborns, open heart surgery is the dominant treatment for large VSDs; however, under certain clinical conditions, a hybrid procedure could be applied to close VSDs. The hybrid procedure is performed while the heart beats and is monitored with TEE. TEE supplies ultrasound images of a high resolution at high frame rates in real time; nevertheless, TEE provides a limited field of view that hinders navigation guidance in the hybrid procedure.

Our main goal was to provide navigation guidance in the hybrid procedure to close VSDs, overcoming limitations with TEE. For navigation guidance, we proposed a virtual environment to monitor maneuvering of surgical instruments in the patient's heart. The virtual environment displays a three-dimensional (3-D) patient-specific heart model, where the VSDs are clearly visible, and virtual models of the surgical instruments. We validated our proposal with retrospective cases of patients with complex VSDs.

We answered three research questions during the development of our study. The first question posed: How to build a physical model of a heart with VSDs to mimic the anatomy and physical properties of a patient-specific heart for palpation, puncture, and ultrasound imaging? We found that PVA-C is an appealing material to build heart phantoms; high water content of PVA-C provides the material with both flexibility for palpation and puncture, and good echogenicity for VSDs characterization in ultrasound imaging.

The second question posed: How to use a 3-D patient-specific heart model for navigation guidance in the hybrid procedure to close VSDs? We found that a landmark registration algorithm is accurate enough to match a 3-D patient-specific virtual heart model and the patient's heart; the virtual model provides 3-D views of the VSDs that facilitate navigation guidance in the hybrid procedure.

The third question stated: How to track motion of a heart with VSDs in ultrasound images to identify the cardiac phase? We found that a particle filter is flexible to include both geometric features of ventricular cavities and intensity values of the ultrasound images from training and test data sets. The filter was robust to blurry boundaries as well as to partial visualization of the ventricles in ultrasound images.

For future work, we recommend: First, the inclusion of a representation of atrioventricular valves in the heart phantoms. Ventricular valves are essential for image interpretation and analysis in echocardiography. Second, the exploration of automatic and semiautomatic methods for segmentation and reconstruction of coronary arteries in diagnostic imaging. Coronary arteries are important landmarks in the physical and virtual heart models for navigation guidance in the hybrid procedure. Third, the evaluation accuracy of the electromagnetic measurement system (EMS) in the operation room. Ferromagnetic materials in the operation room could affect accuracy of the EMS. Fourth, the extension of the particle filtering with machine learning techniques to fully automate the proposed method of heart tracking in ultrasound images. Fifth, the collection of a larger dataset of echocardiographic images from patients with VSDs. A large collection of annotated data is relevant to complement the validation of the proposed methods, with different shapes, heart defects, motion patterns, etc. The introduction of augmented and mixed reality would be highly relevant in the hybrid procedure to close VSDs. Mixing visual information from TEE and several other sources during the hybrid procedure would provide a fully immersive experience for training and planning of treatments. The integration of haptic response might provide additional feedback to immerse the user in the task. Finally, this work can be extended to automate the placement of the needle and the localization of the probe, minimizing risk during the intervention. These extensions would provide further assistance to the cardiologists.

This interdisciplinary project required the combined efforts of a team of engineers and clinicians, working together to bridge a wide variety of expertise into a successful project. The success of this research project relied on good communication between the team members. A constant feedback and evaluation of the proposed methods were important to analyze problems and propose clinically relevant solutions in every step of the process. Additionally, finding solutions to practical problems in the clinical environment, as a interdisciplinary team, was satisfying and rewarding.

APPENDIX I

PUBLICATIONS DURING THE DOCTORAL STUDIES

1. Journals

- **Tibamoso-Pedraza, G.**, Navarro, I., Dion, P., Raboisson, M. J., Lapierre, C., Miró, J., Ratté, S., and Duong, L. (2022). Design of heart phantoms for ultrasound imaging of ventricular septal defects. International journal of computer assisted radiology and surgery, 17(1), 177–184. https://doi.org/10.1007/s11548-021-02406-0
- **Tibamoso-Pedraza, G.**, Amouri, S., Molina, V., Navarro, I., Raboisson, M.-J., Lapierre, C., Miró, J., Ratté, S. and Duong, L. (2022). Navigation guidance for ventricular septal defect closure in heart phantoms. International journal of computer assisted radiology and surgery (under review).

2. Conferences

- **Tibamoso, G.**, Ratté, S. and Duong, L. (2017). Left ventricle wall detection from ultrasound images using shape and appearance information. International Conference Image Analysis and Recognition, pp. 63–70.
- **Tibamoso G.**, Ratté S., Miró J., Duong L. (2018). Automatic characterization of ventricular septal defects from ultrasound images: a preliminary study. 33rd Research Congress of Graduate and Postdoctoral Students in Research at CHU Sainte-Justine, June 8, 2018, Montreal, Canada.

BIBLIOGRAPHY

Alves, N., Kim, A., Tan, J., Hwang, G., Javed, T., Neagu, B. & Courtney, B. K. (2020). Cardiac tissue-mimicking ballistic gel phantom for ultrasound imaging in clinical and research applications. *Ultrasound in Medicine & Biology*, 46(8), 2057–2069.

Amin, Z., Berry, J. M., Foker, J. E., Rocchini, A. P. & Bass, J. L. (1998). Intraoperative closure of muscular ventricular septal defect in a canine model and application of the technique in a baby. *The Journal of thoracic and cardiovascular surgery*, 115(6), 1374–1376.

Anwar, S., Singh, G. K., Miller, J., Sharma, M., Manning, P., Billadello, J. J., Eghtesady, P. & Woodard, P. K. (2018). 3D printing is a transformative technology in congenital heart disease. *JACC: Basic to Translational Science*, 3(2), 294–312.

Balzer, J., Kühl, H., Rassaf, T., Hoffmann, R., Schauerte, P., Kelm, M. & Franke, A. (2008). Real-time transesophageal three-dimensional echocardiography for guidance of percutaneous cardiac interventions: first experience. *Clinical Research in Cardiology*, 97(9), 565–574.

Bhatla, P., Tretter, J. T., Ludomirsky, A., Argilla, M., Latson, L. A., Chakravarti, S., Barker, P. C., Yoo, S.-J., McElhinney, D. B., Wake, N. et al. (2017). Utility and scope of rapid prototyping in patients with complex muscular ventricular septal defects or double-outlet right ventricle: does it alter management decisions? *Pediatric cardiology*, 38(1), 103–114.

Biaggi, P., Fernandez-Golfín, C., Hahn, R. & Corti, R. (2015). Hybrid imaging during transcatheter structural heart interventions. *Current cardiovascular imaging reports*, 8(9), 1–14.

Carneiro, G. & Nascimento, J. C. (2013). Combining multiple dynamic models and deep learning architectures for tracking the left ventricle endocardium in ultrasound data. *IEEE transactions on pattern analysis and machine intelligence*, 99(1), 1.

Crossland, D., Wilkinson, J., Cochrane, A., d'Udekem, Y., Brizard, C. & Lane, G. (2008). Initial results of primary device closure of large muscular ventricular septal defects in early infancy using perventricular access. *Catheterization and Cardiovascular Interventions*, 72(3), 386–391.

Dakkak, W. & Oliver, T. I. (2021). Ventricular septal defect. *StatPearls [Internet]*. Retrieved from: https://www.ncbi.nlm.nih.gov/books/NBK470330/.

Decourt, C. & Duong, L. (2020). Semi-supervised generative adversarial networks for the segmentation of the left ventricle in pediatric MRI. *Computers in Biology & Medicine*, 123, 103884.

Dietenbeck, T., Barbosa, D., Alessandrini, M., Jasaityte, R., Robesyn, V., D'hooge, J., Friboulet, D. & Bernard, O. (2014). Whole myocardium tracking in 2D-echocardiography in multiple orientations using a motion constrained level-set. *Medical image analysis*, 18(3), 500–514.

Faletra, F. F., Ramamurthi, A., Dequarti, M. C., Leo, L. A., Moccetti, T. & Pandian, N. (2014). Artifacts in three-dimensional transesophageal echocardiography. *Journal of the American Society of Echocardiography*, 27(5), 453–462.

Franz, A. M., Haidegger, T., Birkfellner, W., Cleary, K., Peters, T. M. & Maier-Hein, L. (2014). Electromagnetic tracking in medicine—a review of technology, validation, and applications. *IEEE transactions on medical imaging*, 33(8), 1702–1725.

Gustafsson, F. (2015). Particle Filters. In Baillieul, J. & Samad, T. (Eds.), *Encyclopedia of Systems and Control* (pp. 1037–1044). Springer London. doi: https://doi.org/10.1007/978-1-4471-5058-9_66.

Haponiuk, I., Chojnicki, M., Jaworski, R., Steffek, M., Juscinski, J., Sroka, M., Fiszer, R., Sendrowska, A., Gierat-Haponiuk, K. & Maruszewski, B. (2013). Hybrid approach for closure of muscular ventricular septal defects. *Medical science monitor: international medical journal of experimental and clinical research*, 19, 618.

Harold, J. G. (2014). Screening for Critical Congenital Heart Disease in Newborns. *Circulation*, 130(9), e79–e81.

Harrison, C. M. & Gosai, J. N. (2017). Simulation-based training for cardiology procedures: Are we any further forward in evidencing real-world benefits? *Trends in cardiovascular medicine*, 27(3), 163–170.

Horn, B. K. (1987). Closed-form solution of absolute orientation using unit quaternions. *Journal of the Optical Society of America A: Optics and Image Science, and Vision*, 4(4), 629–642.

Jone, P.-N., Ross, M. M., Bracken, J. A., Mulvahill, M. J., Di Maria, M. V. & Fagan, T. E. (2016). Feasibility and Safety of Using a Fused Echocardiography/Fluoroscopy Imaging System in Patients with Congenital Heart Disease. *Journal of the American Society of Echocardiography*, 29(6), 513–521.

Laing, J., Moore, J. T., Vassallo, R., Bainbridge, D., Drangova, M. & Peters, T. M. (2018). Patient-specific cardiac phantom for clinical training and preprocedure surgical planning. *Journal of Medical Imaging*, 5(2), 021222.

Lang, P., Seslija, P., Chu, M. W., Bainbridge, D., Guiraudon, G. M., Jones, D. L. & Peters, T. M. (2012). US–fluoroscopy registration for transcatheter aortic valve implantation. *IEEE Transactions on Biomedical Engineering*, 59(5), 1444–1453.

Laporte, C. & Ménard, L. (2018). Multi-hypothesis tracking of the tongue surface in ultrasound video recordings of normal and impaired speech. *Medical image analysis*, 44, 98–114.

Lasso, A., Heffter, T., Rankin, A., Pinter, C., Ungi, T. & Fichtinger, G. (2014). PLUS: open-source toolkit for ultrasound-guided intervention systems. *IEEE transactions on biomedical engineering*, 61(10), 2527–2537.

Li, F., Chen, M., Qiu, Z., Lu, J. & Wu, W. (2008). A new minimally invasive technique to occlude ventricular septal defect using an occluder device. *The Annals of thoracic surgery*, 85(3), 1067–1071.

Li, F. P., Rajchl, M., Moore, J. & Peters, T. M. (2015). A mitral annulus tracking approach for navigation of off-pump beating heart mitral valve repair. *Medical physics*, 42(1), 456–468.

Linte, C. A., Moore, J., Wedlake, C., Bainbridge, D., Guiraudon, G. M., Jones, D. L. & Peters, T. M. (2009). Inside the beating heart: An in vivo feasibility study on fusing pre-and intra-operative imaging for minimally invasive therapy. *International journal of computer assisted radiology and surgery*, 4(2), 113–123.

Linte, C. A., Davenport, K. P., Cleary, K., Peters, C., Vosburgh, K. G., Navab, N., Jannin, P., Peters, T. M., Holmes, D. R., Robb, R. A. et al. (2013). On mixed reality environments for minimally invasive therapy guidance: Systems architecture, successes and challenges in their implementation from laboratory to clinic. *Computerized Medical Imaging and Graphics*, 37(2), 83–97.

Luo, Z., Cai, J. & Gu, L. (2013). A pilot study on magnetic navigation for transcatheter aortic valve implantation using dynamic aortic model and US image guidance. *International journal of computer assisted radiology and surgery*, 8(4), 677–690.

Marx, G. R. (2014). Transesophageal Three-Dimensional Echocardiography in Congenital Heart Disease. In *Transesophageal Echocardiography for Congenital Heart Disease* (pp. 475–501). Springer.

McLeod, A. J., Currie, M. E., Moore, J. T., Bainbridge, D., Kiaii, B. B., Chu, M. W. & Peters, T. M. (2016). Phantom study of an ultrasound guidance system for transcatheter aortic valve implantation. *Computerized Medical Imaging and Graphics*, 50, 24–30.

Minette, M. S. & Sahn, D. J. (2006). Ventricular septal defects. *Circulation*, 114(20), 2190–2197.

Moore, J. T., Chu, M. W., Kiaii, B., Bainbridge, D., Guiraudon, G., Wedlake, C., Currie, M., Rajchl, M., Patel, R. V. & Peters, T. M. (2013). A navigation platform for guidance of beating heart transapical mitral valve repair. *IEEE Transactions on Biomedical Engineering*, 60(4), 1034–1040.

Morais, P., Tavares, J. M. R., Queirós, S., Veloso, F., D'hooge, J. & Vilaça, J. L. (2017). Development of a patient-specific atrial phantom model for planning and training of inter-atrial interventions. *Medical physics*, 44(11), 5638–5649.

Ouzir, N. L. (2018). *Cardiac motion estimation in ultrasound images using a sparse representation and dictionary learning*. (Ph.D. thesis, Medical Imaging. Université Paul Sabatier – Toulouse III).

Penny, D. J. & Vick, G. W. (2011). Ventricular septal defect. *The Lancet*, 377(9771), 1103–1112.

SickKids staff. (2009). Ventricular septal defect (VSD). Retrieved on January 8, 2022 from: https://www.aboutkidshealth.ca/Article?contentid=1626&language=English.

Sun, Y., Zhu, P., Zhou, P., Guo, Y. & Zheng, S.-Y. (2016). Intra-operative device closure of perimembranous ventricular septal defect without cardiopulmonary bypass under guidance of trans-epicardial echocardiography: a single center experience. *Journal of cardiothoracic surgery*, 11(1), 1.

Surry, K., Austin, H., Fenster, A. & Peters, T. (2004). Poly (vinyl alcohol) cryogel phantoms for use in ultrasound and MR imaging. *Physics in Medicine & Biology*, 49(24), 5529.

Thaden, J. J., Sanon, S., Geske, J. B., Eleid, M. F., Nijhof, N., Malouf, J. F., Rihal, C. S. & Bruce, C. J. (2016). Echocardiographic and Fluoroscopic Fusion Imaging for Procedural Guidance: An Overview and Early Clinical Experience. *Journal of the American Society of Echocardiography*, 29(6), 503–512.

Thakkar, B., Patel, N., Shah, S., Poptani, V., Madan, T., Shah, C., Shukla, A. & Prajapati, V. (2012). Perventricular device closure of isolated muscular ventricular septal defect in infants: A single centre experience. *Indian heart journal*, 64(6), 559–567.

Tibamoso, G., Ratté, S. & Duong, L. (2017). Left ventricle wall detection from ultrasound images using shape and appearance information. *International Conference Image Analysis and Recognition*, pp. 63–70.

Tibamoso-Pedraza, G., Navarro, I., Dion, P., Raboisson, M.-J., Lapierre, C., Miró, J., Ratté, S. & Duong, L. (2022). Design of heart phantoms for ultrasound imaging of ventricular septal defects. *International journal of computer assisted radiology and surgery*, 17, 177–184. doi: https://doi.org/10.1007/s11548-021-02406-0.

Ungi, T., Lasso, A. & Fichtinger, G. (2016). Open-source platforms for navigated image-guided interventions. *Medical Image Analysis*, 33, 181–186. Retrieved from: http://dx.doi.org/10.1016/j.media.2016.06.011.

Wan, W., Campbell, G., Zhang, Z., Hui, A. & Boughner, D. (2002). Optimizing the tensile properties of polyvinyl alcohol hydrogel for the construction of a bioprosthetic heart valve stent. *Journal of Biomedical Materials Research: An Official Journal of the Society for Biomaterials, the Japanese Society for Biomaterials, and the Australian Society for Biomaterials and the Korean Society for Biomaterials*, 63(6), 854–861.

Xing, Q., Pan, S., An, Q., Zhang, Z., Li, J., Li, F., Wu, Q. & Zhuang, Z. (2010). Minimally invasive perventricular device closure of perimembranous ventricular septal defect without cardiopulmonary bypass: multicenter experience and mid-term follow-up. *The Journal of thoracic and cardiovascular surgery*, 139(6), 1409–1415.

Yamada, T., Osaka, M., Uchimuro, T., Yoon, R., Morikawa, T., Sugimoto, M., Suda, H. & Shimizu, H. (2017). Three-dimensional printing of life-like models for simulation and training of minimally invasive cardiac surgery. *Innovations*, 12(6), 459–465.

Yin, S., Zhu, D., Lin, K. & An, Q. (2014). Perventricular device closure of congenital ventricular septal defects. *Journal of cardiac surgery*, 29(3), 390–400.